UNIVERSIDADE ESTADUAL DE CAMPINAS
Faculdade de Engenharia Elétrica e de Computação

Claudio Alfonso Bohorquez Camargo

Probability of Detection in Conventional AOA Using ULA and URA Arrays

Probabilidade de Detecção em AOA Convencional Usando Arranjos ULA e URA.

Campinas

2018

UNIVERSIDADE ESTADUAL DE CAMPINAS
Faculdade de Engenharia Elétrica e de Computação

Claudio Alfonso Bohorquez Camargo

Probability of Detection in Conventional AOA Using ULA and URA Arrays

Probabilidade de Detecção em AOA Convencional Usando Arranjos ULA e URA.

Dissertation presented to the Faculty of Electrical and Computer Engineering of the University of Campinas in partial fulfillment of the requirements for the degree of Master, in the area of Telecommunications and Telematics.
Dissertação apresentada à Faculdade de Engenharia Elétrica e de Computação da Universidade Estadual de Campinas como parte dos requisitos exigidos para a obtenção do título de Mestre em Engenharia Elétrica, na Área de Telecomunicações e Telemática.

Supervisor: Prof. Dr. Gustavo Fraidenraich

Este exemplar corresponde à versão final da tese defendida pelo aluno Claudio Alfonso Bohorquez Camargo, e orientada pelo Prof. Dr. Gustavo Fraidenraich

---

Campinas

2018

Agência(s) de fomento e nº(s) de processo(s): CAPES

Ficha catalográfica
Universidade Estadual de Campinas
Biblioteca da Área de Engenharia e Arquitetura
Rose Meire da Silva - CRB 8/5974

B635p

Bohorquez Camargo, Claudio Alfonso, 1988-
Probability of detection in conventional AOA using ULA and URA arrays / Claudio Alfonso Bohoquez Camargo. – Campinas, SP : [s.n.], 2018.

Orientador: Gustavo Fraidenraich.
Dissertação (mestrado) – Universidade Estadual de Campinas, Faculdade de Engenharia Elétrica e de Computação.

1. Canal de desvanecimento. 2. Radio - Transmissores e transmissão -Desvanecimento. 3. Sistemas MIMO. 4. sistemas de comunicação sem fio. 5. Telecomunicações - Codificação. I. Fraidenraich, Gustavo, 1975-. II. Universidade Estadual de Campinas. Faculdade de Engenharia Elétrica e de Computação. III. Título.

Informações para Biblioteca Digital

Título em outro idioma: Probabilidade de detecção em AOA convencional usando arranjos ULA e URA
Palavras-chave em inglês:
Fading channel
Radio - Transmitters and Transmission - Fading
MIMO systems
Wireless communication systems
Telecommunications - Codification
Área de concentração: Telecomunicações e Telemática
Titulação: Mestre em Engenharia Elétrica
Banca examinadora:
Gustavo Fraidenraich [Orientador]
Paulo Cardieri
Richard Demo Souza
Data de defesa: 24-08-2018
Programa de Pós-Graduação: Engenharia Elétrica

COMISSÃO JULGADORA-DISSERTAÇÃO DE MESTRADO

Candidato: Claudio Alfonso Bohorquez Camargo. RA: 163666.

Data de Defesa: 24 de Agosto de 2018.

Título da Tese: "Probability of Detection in Conventional AOA Using ULA and URA Arrays (Probabilidade de Detecção em AOA Convencional Usando Arranjos ULA e URA)".

Prof. Dr. Gustavo Fraidenraich (Presidente, FEEC/ UNICAMP)

Prof. Dr. Paulo Cardieri (FEEC/ UNICAMP)

Prof. Dr. Richard Demo Souza (UFSC)

A ata de defesa, com as respectivas assinaturas dos membros da Comissão Julgadora, encontra-se no SIGA (Sistema de Fluxo de Dissertaçã o/Tese) e na Secretaria de Pós-Graduação da Faculdade de Engenharia Elétrica e de Computação.

Dedico esta tese à minha família, meus amigos e minha namorada.

Acknowledgements

I am thankful to life-nature-God-energy for allowing me to achieve a master's degree.

I thank my parents Claudio and Luz Marina and my sister Samia for supporting me in all projects that I develop.

I acknowledge my girlfriend Natalia for her company in this process.

I am thankful to all my friends of the State University of Campinas (UNICAMP) for helping and joining me on this path, especially Ruby, Melissa, Yalena, Dimas Augusto, Camilo, Loren, and Laura.

I thank my master's supervisor, professor Gustavo Fraidenraich, for having accepted, guided and corrected me in the achievement of the master's degree.

Special thanks to the Qualifying and Examining Committee members, professors Paulo Cardieri, Michel Yacoub,and Richard Demo for evaluating and giving feedback on the work.

Last but not least, I would like to thank CAPES for its financial support.

*"**Imagen**:*
El Fuego. En sí mismo no tiene fuerza: depende de su medio. Dale aire, madera seca, viento que avive la flama y adquirirá un impulso aterrador, se desatará, se alimentará a si mismo, consumirá todo a su paso. Nunca dejes ese poder al azar."
Robert Greene. (GREENE, 2007)

Abstract

In Massive Multiple Input Multiple Output (MIMO) systems, where a large number of antennas is used, the dependency of the power spectrum on the signal direction allows Angle of Arrival (AoA) estimation with a very high precision. In this work, we derive the probability to correctly detect the angle of arrival using the conventional beamformer. The derivation is presented in an exact manner for Uniform Linear Array (ULA) and Uniform Rectangular Array (URA) geometries. The resulting expressions depend on the noise power, Line of Sight Component (LoS) (modeled as the fading mean), fading variance, number of signal snapshots, number of steering angles, and the number of antennas. We have numerically evaluated the simulated and analytical probability of detection and they have shown a perfect agreement for distinct scenarios framed in the Massive MIMO condition.

Keywords: Fading channel; Radio - Transmitters and Transmission - Fading; MIMO Systems; Wireless Communication Systems; Telecommunications - Codification; Angle of Arrival; Beamforming; Probability of Detection; ULA; URA.

Resumo

Em sistemas de MIMO massivo, onde um grande número de antenas é usado, a dependência do espectro de energia na direção do sinal permite estimar o AoA com uma precisão muito alta. Neste trabalho, derivamos a probabilidade de detectar corretamente o ângulo de chegada usando o *beamformer* convencional. A derivação é apresentada de uma maneira exata para as geometrias ULA e URA. As expressões resultantes dependem da potência do ruído, a linha de visada (modelada como a média de desvanecimento), variância de desvanecimento, número de amostras do sinal, número de ângulos de orientação e o número de antenas. Avaliamos numericamente a probabilidade de detecção simulada e analítica e elas mostraram uma concordância perfeita para cenários distintos enquadrados na condição de MIMO massivo.

Palavras-chaves: Canal de Desvanecimento; Radio - Transmissores e transmissão - Desvanecimento; Sistemas MIMO; Sistemas de Comunicação sem fio; Telecomunicações - Codificação; Ângulo de chegada; Beamforming; Probabilidade de Detecção; ULA; URA.

Acronyms

AoA - Angle of Arrival.

CCU - Central Communications Unit.

CDF - Cumulative Distribution Function.

C-RAN - Centralized Radio Access Network.

CSI - Channel State Information.

D2D - Device to Device Communications.

DOI - Digital Object Identifier.

LoS - Line of Sight Component.

ESPRIT - Estimation of Signal Parameters via Rotational Invariance Technique.

MIMO - Multiple Input Multiple Output.

MUSIC - Multiple Signal Classification.

PDF - Probability Density Function.

RBS - Radio Base Station.

RMSE - Root Mean Squared Error.

RSS - Received Signal Strength.

SNR - Signal to Noise Ratio.

ToA - Time of Arrival.

UCA - Uniform Circular Array.

UCyA - Uniform Cylindrical Array.

ULA - Uniform Linear Array.

UNICAMP - State University of Campinas.

URA - Uniform Rectangular Array.

Symbols

ψ - Azimuth angle.

ϕ - Azimuth AoA of dedicated signal.

δ - Distance between elements of array.

ξ - Elevation angle.

θ - Elevation AoA of dedicated signal.

$\Im(.)$ - Imaginary component operator.

L - Fading mean Component.

$\mathbf{E}[.]$ - Mean operator.

σ_n - Noise standard deviation.

σ_n^2 - Noise power or Noise variance.

M - Number of Antennas in ULA.

M_x - Number of x axis Antennas in URA.

M_y - Number of y axis Antennas in URA.

N - Number of Radio Base Stations (RBSs).

K - Number of Snapshots.

σ_f - Rice (Rayleigh) standard deviation.

σ_f^2 - Rice (Rayleigh) fading variance.

$\Re(.)$ - Real component operator.

λ - Signal wavelength.

$\mathbf{var}[.]$ - Variance operator.

List of Figures

List of Tables

Table of contents

1 Introduction

The upcoming fifth generation (5G) of mobile network communication technology is considering the use of Massive MIMO, that is, the use of a large number of antennas at the base station. Although wireless communications and Massive MIMO research have required a significant amount of effort at architecture, channel modeling, performance analysis, power allocation, parallel models (Device to Device Communications (D2D)) and Channel State Information (CSI) (LARSSON *et al.*, 2014; XU *et al.*, 2017a; XU *et al.*, 2017b; MARZETTA, 2010), there are few works (GARCIA *et al.*, 2017) where a Massive MIMO system is used for localization of terminals.

There are several techniques for device localization, among the most important we can enumerate the following:

- **Time of Arrival (Time of Arrival (ToA))**, which uses the delay principle in signal transmission and matched filter for time/distance estimation (DARDARI *et al.*, 2008).
- **Angle of Arrival (AoA)**, which uses the signal delay between elements of an antenna array and/or the correlation of power and direction of arrival of a group of signals (CHEN *et al.*, 2010; WANG *et al.*, 2016; HE, 2014; FAN *et al.*, 2018).
- **Received Signal Strength (Received Signal Strength (RSS))**, which uses the relationship between distance and power of a signal transmitted in a physical medium (ZEYTINCI *et al.*, 2013; SAVIC; LARSSON, 2015).
- **Hybrid approaches**, which employ simultaneous available data from previously mentioned methods to determine the direction of arrival estimation (GARCIA *et al.*, 2017; KHAN *et al.*, 2014).

Usually, all the described approaches work as inputs for localization applications where the final output is a position or a distance. Typical works in these applications investigate the development of new algorithms using procedures like Least Squares (BECK *et al.*, 2008), Kalman filters (ZHANG *et al.*, 2013) or fingerprint methods (FANG; WANG, 2011). In the mentioned cases, the performance is assessed using metrics like position/angle Root Mean Squared Error (RMSE) versus signal to noise ratio, number of antennas, or bias (DARDARI *et al.*, 2008).

1.1 Objective: Justification and Contribution

Massive MIMO takes advantage from the large number of antennas to decrease the effect of noise and fading (LARSSON *et al.*, 2014). In the Marzetta's (MARZETTA, 2010) pioneer paper, it has been shown that the use of the conventional beamforming technique is optimal as the number of antennas increases. It turns out that this basic technique for AoA estimation is the same used for combining the signals in the Massive MIMO system. Therefore, our derivation can be used in both contexts (combining signals and AoA estimation with conventional beamforming).

Several works have proposed algorithms and assessment methods for AoA estimation (CHEN *et al.*, 2010; WANG *et al.*, 2016; HE, 2014; FAN *et al.*, 2018; BECK *et al.*, 2008; ZHANG *et al.*, 2013) , however, to the best of our knowledge, the probability of detection for AoA appraisal using the conventional beamformer is unavailable in the literature.

There are other AoA estimation techniques such as Capon (CAPON, 1969), Multiple Signal Classification (MUSIC (SCHMIDT, 1986), Estimation of Signal Parameters via Rotational Invariance Technique (ESPRIT) (ROY; KAILATH, 1989) , and RiMax (SALMI; MOLISCH, 2011) that present better performance than the basic method investigated here. However, the connection to Massive MIMO technique plays a key role that has motivated the derivation of the proposed metric. In fact, we have also tried to derive the same metric for MUSIC and Capon techniques, however, these calculations are quite involved and would require new developments in invertible non-central complex Wishart matrices, supersymmetry (use of anticommuting variables) and complex eigenvectors PDFs (CHEN *et al.*, 2010; MUIRHEAD, 2005). In this way, we can say our derived expressions can be used as a lower bound or an approximation to estimate the probability of detection for Capon and MUSIC techniques.

The objective in this work is to derive the probability of detection (as a new metric) for AoA using conventional beamforming in fading and noise scenarios for ULA and URA geometries. Our derived expressions are presented as a function of the number of signal snapshots, the magnitude of the fading mean (LoS), the magnitude of fading variance, the magnitude of noise variance, the number of steering angles and the number of antennas.

1.2 Organization of the thesis

The thesis is organized as follows:

- The current Introduction presents and sets the objective of this work.
- Chapter 2 depicts the system model and selected AoA algorithms.
- Chapter 3 shows the derived expressions of the equivalent random variable for a conventional beamforming technique using ULA and URA geometries. This equivalent random variable is an entry for the probability of detection expression.
- Chapter 4 exhibits numerical results (analytical and simulated) of the previous deducted random variable.
- Chapter 5 shows the formulation and derivation of the probability of detection. Moreover, simulated and analytical results are exposed and discussed.
- Conclusions section draws the conclusions and proposed future work for the presented developments.

2 System Model

Chapter 2 exposes the system model used in this work and selected algorithms for evaluation.

2.1 System Model

The system is framed in a scenario where the next assumptions are established as stated in (KRIM; VIBERG, 1996) and (CHEN *et al.*, 2010):

- **Isotropic and Linear Transmission Medium**: The physical medium maintains is properties in all possible directions and can be superimposed linearly at any point. This ensures steadiness in wave propagation (Despite AoA) and linearity in the system processing at the receiver.
- **Far Field**: The wavefront of the signal is planar and arrives at the receiver in the same AoA for all the array elements due to their location in such a distance that guarantees far field approximation (received signals are parallel).
- **AWGN Channel**: The channel has a noise modeled as a complex white Gaussian process.
- **Rice Channel**: The channel fading is modeled as a non-negative mean (modeling the LoS component) complex Gaussian process.

With the assumptions set, Fig. 2.1 shows a typical ULA system where the signal received by the i-th antenna element is given as:

$$r_i(t) = s(t)h_i(t)e^{j(i-1)\mu(\theta)} + n_i(t), \tag{2.1}$$

where $s(t)$ is the transmitted signal, $\mu(\theta) = \frac{2\pi}{\lambda}\Delta\sin(\theta)$ is the spatial frequency, $h_i(t)$ models the fading, λ is the wavelength, Δ is the distance between the elements (usually modeled as $\Delta = \frac{\lambda}{2}$), θ is the angle of arrival, and $n_i(t)$ is the additive Gaussian noise.

The signal received by all the elements of the array can be written in a $1 \times M$ vector form as:

$$\mathbf{r}(t) = \mathbf{a}(\theta) \circ \mathbf{h}(t)s(t) + \mathbf{n}(t), \tag{2.2}$$

where the symbol $\circ$ stands for the Hadamard product, and the components are:

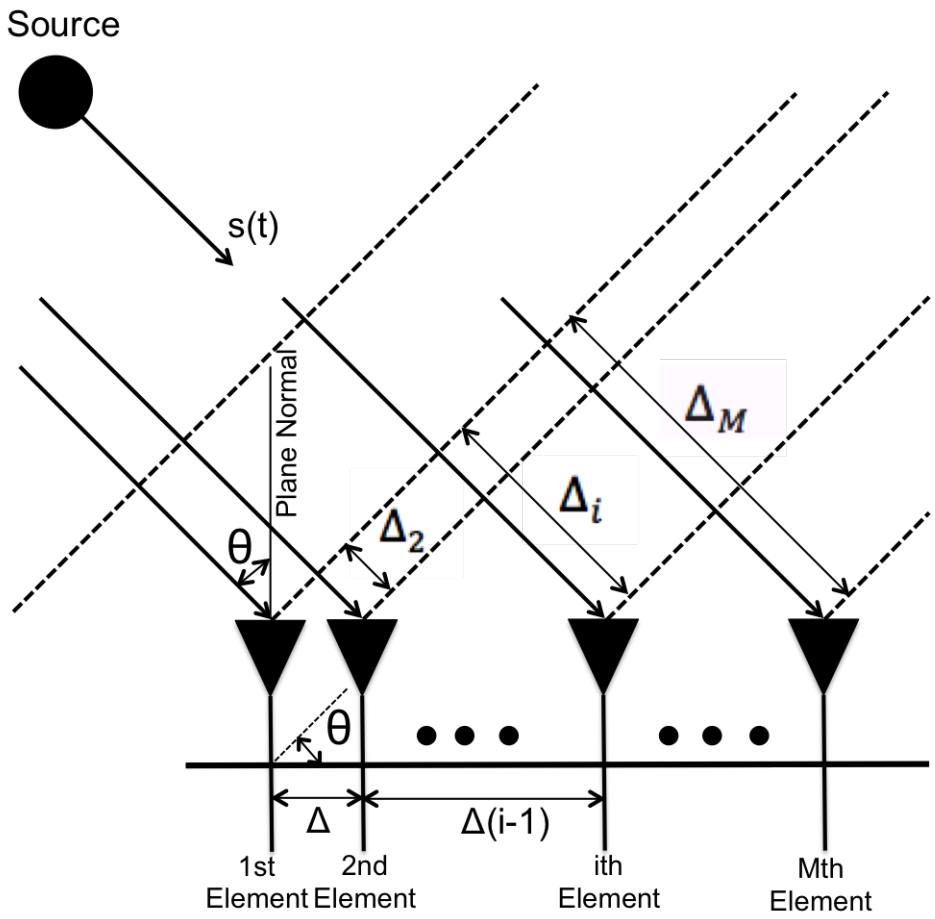

Figure 2.1 – Physical model of an ULA system with M antennas. Based on (CHEN *et al.*, 2010)

- Steering vector $\mathbf{a}(\theta)$, given as:

$$\mathbf{a}(\theta) = \begin{bmatrix} 1 & e^{j\mu(\theta)} & \dots & e^{j(M-1)\mu(\theta))} \end{bmatrix}, \tag{2.3}$$

- The fading vector $\mathbf{h}(t)$ is a complex Gaussian random process with mean $\mu_f = L/\sqrt{2}$ for the real and imaginary part ($L/\sqrt{2}$ is assumed as the fading mean component and models the dominant LoS component), and covariance matrix $\sigma_f^2\mathbf{I}_M$, where $\mathbf{I}_M$ stands for a $M \times M$ identity matrix. Namely, the channel for signal $s(t)$ is set as Rician fading with a dominant LoS component, i.e. μ_f.

- The noise $\mathbf{n}(t)$ is a complex random process with zero mean and covariance matrix $\sigma_n^2\mathbf{I}$.

2.1.1 URA Case

URA configuration uses an extra angle dimension where the array is located at the xy plane, with the first element placed at the origin (see Fig. 2.2 and Fig. 2.3). In

this way, the elevation and azimuth steering vectors of the impinging signal in the array are given as:

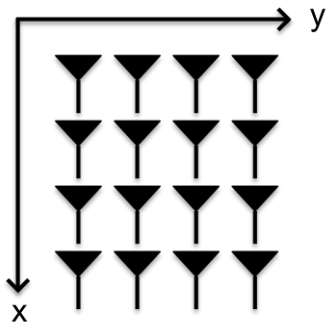

Figure 2.2 – URA Configuration.

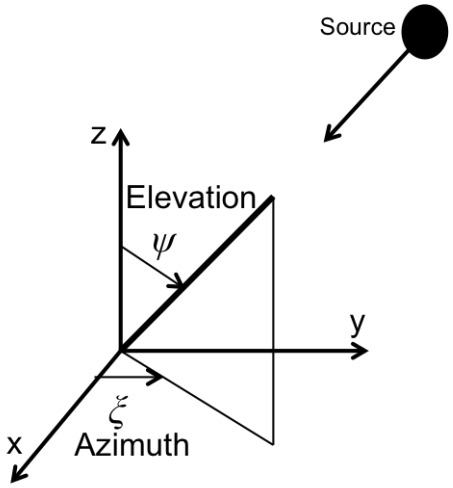

Figure 2.3 – Elevation and Azimuth angles in URA layout.

$$\mathbf{a}_u(\psi,\xi) = \begin{bmatrix} 1 & e^{ju} & ... & e^{j(M_x-1)u} \end{bmatrix}, \tag{2.4}$$

$$\mathbf{a}_v(\psi,\xi) = \begin{bmatrix} 1 & e^{jv} & ... & e^{j(M_y-1)v} \end{bmatrix}, \tag{2.5}$$

where

$$u = -(2\pi/\lambda)\Delta \sin(\psi)\sin(\xi), \tag{2.6}$$

and

$$v = -(2\pi/\lambda)\Delta \sin(\psi)\cos(\xi). \tag{2.7}$$

These vectors are multiplied to get a matrix $\mathbf{A}(\psi,\xi)$ as:

$$\mathbf{A}(\psi,\xi) = \mathbf{a}_v^H(\psi,\xi)\mathbf{a}_u(\psi,\xi). \tag{2.8}$$

Then matrix $\mathbf{A}(\psi,\xi)$ is transformed into a $1 \times M_xM_y$ vector using the vec $(\cdot)$ operation:

$$\mathbf{a}(\psi,\xi) = \text{vec}\left[\mathbf{A}(\psi,\xi)\right]. \tag{2.9}$$

Remember, that the vec $(\cdot)$ operator is a two step operation on a matrix: first, it concatenates the columns of a matrix in a single column vector of size $M_x M_y \times 1$, and then it transposes this vector into a line vector of size $1 \times M_x M_y$. Note that, from (2.2) and (2.9), $\mathbf{r}_k$ has the same dimension as $\mathbf{a}(\psi, \xi)$, therefore the size of $\mathbf{r}_k$ for URA case will be $1 \times M_x M_y$.

2.2 AoA algorithms

Covariance matrix calculates the degree of correlation of a group of signals. The higher the value of the matrix elements, the higher the degree of correlation between the signals. Noise is usually uncorrelated (as modeled in this work), opposite to a group of signals coming from the same origin, which are highly correlated. In this case, the high value of correlation comes from the fact that the signals are essentially the same with some delay, in other words, they are closely alike between them. Therefore the sample covariance matrix $\mathbf{R}$ can be used to estimate the angle of arrival, as vastly reported in many references (CHEN *et al.*, 2010; XU *et al.*, 1994; JONG; HERBEN, 1999; KWAKKERNAAT *et al.*, 2008).

Assuming a specific time, we can define $\mathbf{r}_k = \mathbf{r}(t = t_k)$, and therefore the spatial covariance matrix can be defined as:

$$\mathbf{R} = \frac{1}{K} \sum_{k=0}^{K-1} \mathbf{r}_k^H \mathbf{r}_k, \tag{2.10}$$

where $(\cdot)^H$ stands for the conjugate transpose or Hermitian operator. The variable K is the number of snapshots taken to the signal. Different AoA algorithms use and process in a particular way the information that is given by the covariance matrix $\mathbf{R}$ as shown in following subsections. Finally, for URA case, the dimension of covariance matrix $\mathbf{R}$ will be given as $M_x M_y \times M_x M_y$.

2.2.1 Conventional Beamforming

The conventional beamformer method estimates the spatial power spectrum for every possible AoA frequency as (CHEN *et al.*, 2010, Eq. 3.43):

$$H_{ULA-CON}(\psi) = \frac{\mathbf{a}(\psi)\mathbf{R}\mathbf{a}^H(\psi)}{\mathbf{a}(\psi)\mathbf{a}^H(\psi)}, \tag{2.11}$$

where $\mathbf{a}(\psi)$ is the steering vector for all possible AoA, as defined in (2.3). The angle variable ψ is discretized into Q possible values, in other words there are Q steering frequencies. When the condition $\psi = \theta$ occurs, (2.11) reaches its maximum, which is the key assumption to estimate θ (the AoA of the direct line of sight component). Is is important

to note that the original AoA θ will be covered by one the closest value of the Q steering angles. However as the number of Q possible angles increases (which is the case for Massive MIMO), the error associated with this discretization will be negligible.
For all of the snapshots, the numerator can be given as:

$$\mathbf{a}(\theta)\mathbf{r}_k^H\mathbf{r}_k\mathbf{a}^H(\theta) = \overline{\mathbf{q}_k}\mathbf{q}_k = |\mathbf{q}_k|^2. \tag{2.12}$$

where $\mathbf{q}_k = \mathbf{r}_k\mathbf{a}^H(\theta)$.

Note that (2.12) presents the term $\mathbf{q}_k = \mathbf{r}_k\mathbf{a}^H(\theta)$, that is exactly the spatial implementation of the Maximal Ratio Combining (MRC) principle (MARZETTA, 2010), in which $\mathbf{a}^H(\theta)$ is the spatial channel coefficient that optimizes the combining of the received signal $\mathbf{r}_k$. It is noteworthy to emphasize the following: The MRC technique has been devised as the optimal combining technique since it maximizes the signal to noise ratio at the combiner output. In the Massive MIMO context, this method has been used since the effect of the noise and fast fading vanish as the number of antennas is very large (LARSSON *et al.*, 2014).

Other useful interpretation for (2.11) is the matched filter principle: a received signal is correlated with its template signal. The filter response is maximum when both signals are similar (i.e. correlated). In this particular case (2.11) could be seen as a spatial matching filter that gives a maximum response when the impinging signals (characterized on $\mathbf{R}$) match with the steering vector of the angle of origin $\mathbf{a}(\theta)$.

For URA case, the power spatial spectrum is defined as:

$$H_{URA-CON}(\psi,\xi) = \frac{\mathbf{a}(\psi,\xi)\mathbf{R}\mathbf{a}^H(\psi,\xi)}{\mathbf{a}(\psi,\xi)\mathbf{a}^H(\psi,\xi)}, \tag{2.13}$$

and in the same fashion as (2.11), (2.13) achieves its maximum when $(\psi = \theta, \xi = \phi)$, which is the AoA of the signal.

2.2.2 Capon Beamforming

Capon beamforming principle works on an inverse approach (CHEN *et al.*, 2010; CAPON, 1969): it forms a beam in the AoA direction and forms nulls in other directions to dismiss other signals. This is achieved by restricting the beam in the AoA direction (maintaining unity gain) and minimizing the array output power on the other directions. This issue, results in a power spectrum for Capon Beamforming:

$$H_{ULA-CAP}(\psi) = \frac{1}{\mathbf{a}(\psi)\mathbf{R}^{-1}\mathbf{a}^H(\psi)}, \tag{2.14}$$

Once again, the angle variable ψ is discretized into Q possible values, in other words there are Q steering frequencies, and when the condition $\psi = \theta$ occurs, (2.14) reaches

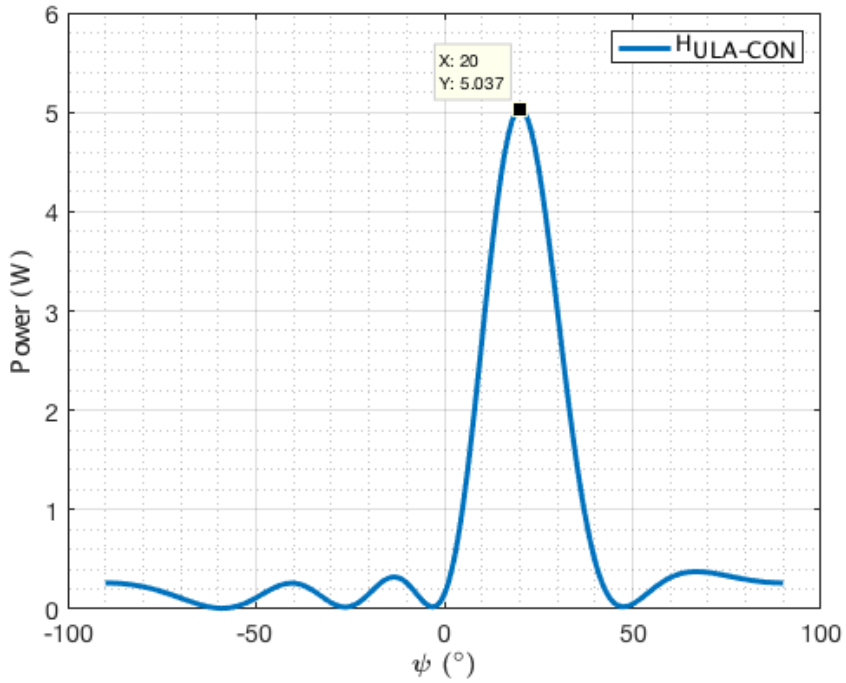

Figure 2.4 – Power spectrum vs angle ψ for Conventional beamforming with $\theta = 20°$, $K = 5$, $L = 1$, $M = 5$, Q=181 ($\Delta_\psi = 1.0°$), $\sigma_n = 0.1$ and $\sigma_f = 0.1$ in ULA configuration.

its maximum, which is the key assumption to estimate θ. This method proves to have a higher computational cost due to the calculation of the inverse matrix where the greater the number of array elements, the severer the computing time and power. For URA case, the power spatial spectrum is defined as:

$$H_{URA-CAP}(\psi, \xi) = \frac{1}{\mathbf{a}(\psi, \xi)\mathbf{R}^{-1}\mathbf{a}^H(\psi, \xi)}, \tag{2.15}$$

and in the same fashion as (2.14), (2.15) achieves its maximum when $(\psi = \theta, \xi = \phi)$, which is the AoA of the signal.

At last, it is worth to remember that number of snapshots K in covariance matrix $\mathbf{R}$ of (2.4) inserted in equations (2.14) and (2.15) shall always be greater or equal to the number of antennas M, ($K \geq M$ or $K \geq M_x M_y$), in order to avoid singularity in the matrix that impedes the existence of invertible matrix, i. e. the basis of Capon method.

2.2.3 MUSIC

MUSIC (SCHMIDT, 1986) method is framed into the subspace techniques, that relies on the covariance matrix $\mathbf{R}$ space whose properties are given as (CHEN *et al.*, 2010):

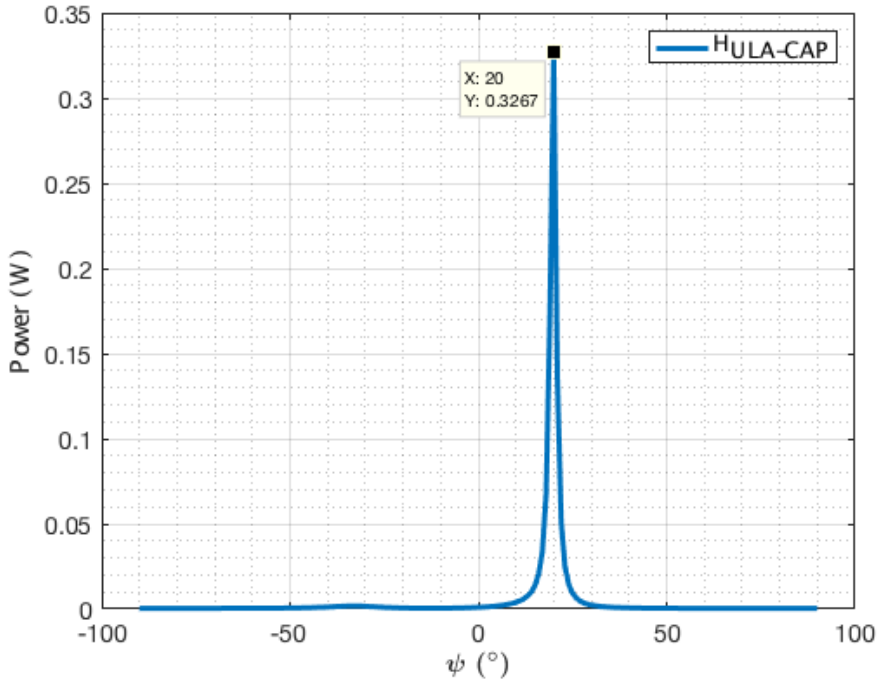

Figure 2.5 – Power spectrum vs angle ψ for Capon beamforming with $\theta = 20°$, $K = 5$, $L = 1$, $M = 5$, Q=181 ($\Delta_\psi = 1.0°$), $\sigma_n = 0.1$ and $\sigma_f = 0.1$ in ULA configuration.

1. The signal space, spanned by its eigenvectors, can be partitioned into two orthogonal subspaces, namely the signal subspace and noise subspace (CHEN *et al.*, 2010).
2. The steering vector corresponds to the signal subspace (CHEN *et al.*, 2010).
3. The noise subspace is spanned by the eigenvectors associated with the smallest eigenvalues of the correlation matrix (covariance) (CHEN *et al.*, 2010).
4. The signal subspace is spanned by the eigenvectors associated with the largest eigenvalue (CHEN *et al.*, 2010).

With this basis, MUSIC algorithm is given as:

1. Calculate covariance matrix $\mathbf{R}$
2. Develop eigen-decomposition on $\mathbf{R}$:

$$\mathbf{RW} = \mathbf{W}\Upsilon \tag{2.16}$$

   Where $\Upsilon = diag[\upsilon_0, \upsilon_1, \ldots, \upsilon_{M-1}]$ are the eigenvalues of $\mathbf{R}$ and $\mathbf{W}$ is the matrix that contains all the eigenvectors associated to $\mathbf{R}$.

3. Find the largest eigenvalue υ_{MAX}. In (SCHMIDT, 1986) was proven that the eigenvectors associated to υ_{MAX} spanned the signal subspace.

4. Remove column of eigenvectors associated to υ_{MAX} in $\mathbf{W}$. Now $\mathbf{W}$ turns into $\mathbf{W}_n$, size $M \times M-1$.

5. Calculate the power spectrum with the inverse approach, using matrix $\mathbf{W}_n$:

$$H_{ULA-MUS}(\psi) = \frac{1}{\mathbf{a}(\psi)\mathbf{W}_n\mathbf{W}_n^H\mathbf{a}^H(\psi)}, \tag{2.17}$$

   The eigenvectors in $\mathbf{W}_n$ are spanning the noise subspace, therefore they will produce nulls in the denominator of (2.17) when $\psi = \theta$ (due to the orthogonality between signal and noise subspaces). Subsequently, this product is inverted to obtain the peaks in the spectrum, which determines the associated AoA, θ. Once again, the angle variable ψ is discretized into Q possible values, in other words there are Q steering frequencies.

For URA case, the algorithm remains the same, and the power spatial spectrum is defined as:

$$H_{URA-MUS}(\psi,\xi) = \frac{1}{\mathbf{a}(\psi,\xi)\mathbf{W}_n^H\mathbf{W}_n\mathbf{a}^H(\psi,\xi)}, \tag{2.18}$$

and in the same fashion as (2.17), equation (2.18) achieves its maximum when $(\psi = \theta, \xi = \phi)$, which is the AoA of the signal.

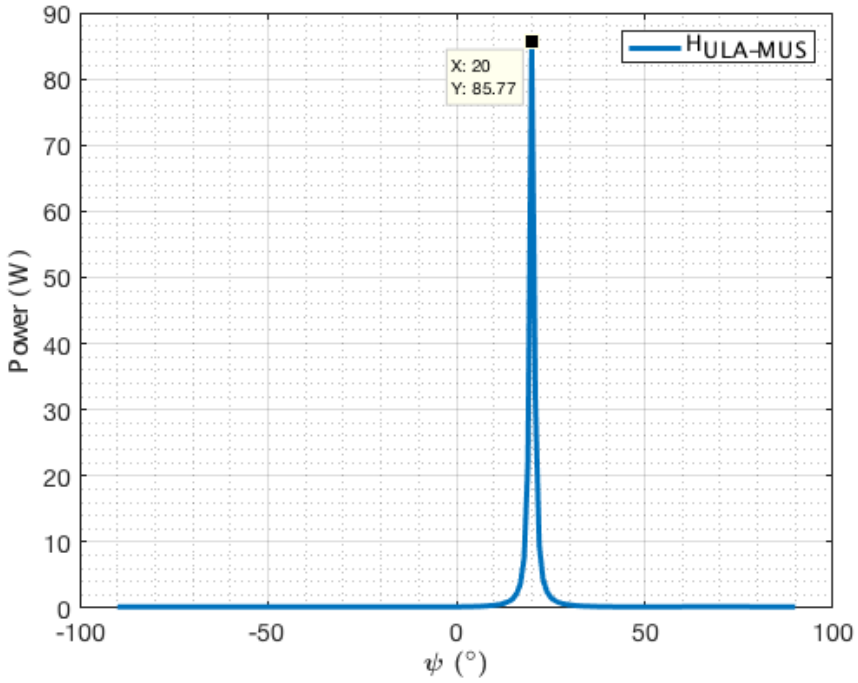

Figure 2.6 – Power spectrum vs angle ψ for MUSIC beamforming with $\theta = 20°$, $K = 5$, $L = 1$, $M = 5$, Q=181 ($\Delta_\psi = 1.0°$), $\sigma_n = 0.1$ and $\sigma_f = 0.1$ in ULA configuration.

2.2.4 Maximum Likelihood

The maximum likelihood principle is a universal estimation technique where the objective is to find the model (set of equations and/or their parameters) or just the parameters (when the model is known) that fits the best with observed data. To do so, for every possible model or group of parameters, the estimator calculates a selected metric (typically the error or the squared error) and chooses the model that minimizes the metric itself. Because some models could be massive, complex or with a wide span of the parameters, the maximum likelihood technique is computationally intensive, however, it always has the best performance in terms of error.

For this application, in particular, the estimator is formulated in the least squares (LS) form as (CHEN *et al.*, 2010):

$$\hat{\theta} = \arg\min_{\theta,\hat{s}(t)} \langle \left\| \mathbf{r}(t_n) - \mathbf{a}(\hat{\theta})\hat{s}(t_n) \right\|^2 \rangle_N \tag{2.19}$$

where the estimated angle $\hat{\theta}$, is the one that minimizes the LS fit of a group of possible steering vectors and reconstructed signals.The angle variable is discretized into Q possible values. Therefore $\hat{\theta}$ is the associated angle of the minimum value for the Q possible values of the cost function

$$J = \langle \left\| \mathbf{r}(t_n) - \mathbf{a}(\hat{\theta})\hat{s}(t_n) \right\|^2 . \rangle_N \tag{2.20}$$

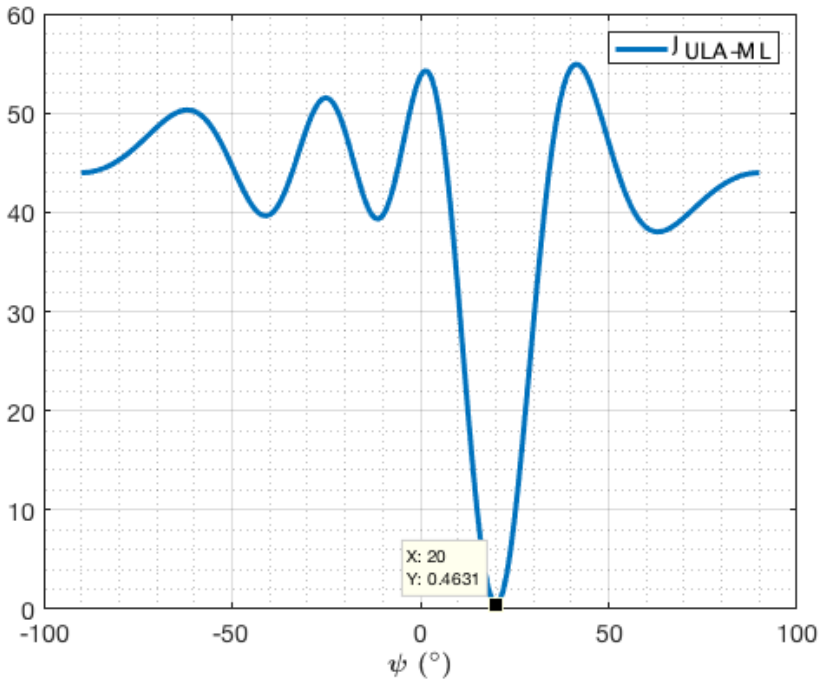

Figure 2.7 – Cost Function vs angle ψ for Conventional beamforming with $\theta = 20°$, $K = 5$, $L = 1$, $M = 5$, Q=181 ($\Delta_\psi = 1.0°$), $\sigma_n = 0.1$ and $\sigma_f = 0.1$ in ULA configuration.

2.3 AoA Estimation performance

In order to show the performance of the presented methods, we simulated the estimated angle RMSE, estimated angle mean $\mu_{\hat{\theta}}$ and estimated angle standard deviation $\sigma_{\hat{\theta}}$, as shown in Fig. 2.8 and Fig. 2.9. These metrics are calculated as:

$$\text{RMSE} = \sqrt{\mathbf{E}\left[\left(\theta - \hat{\theta}\right)^2\right]} \tag{2.21}$$

$$\mu_{\hat{\theta}} = \mathbf{E}\left[\hat{\theta}\right] \tag{2.22}$$

$$\sigma_{\hat{\theta}} = \sqrt{\mathbf{var}\left[\hat{\theta}\right]} \tag{2.23}$$

where θ is the correct angle used in the simulation and $\hat{\theta}$ is the estimated angle. The mean operator $\mathbf{E}[\cdot]$ and the variance operator $\mathbf{var}[\cdot]$ compute the average and variance over many realizations of the Monte Carlo simulation.

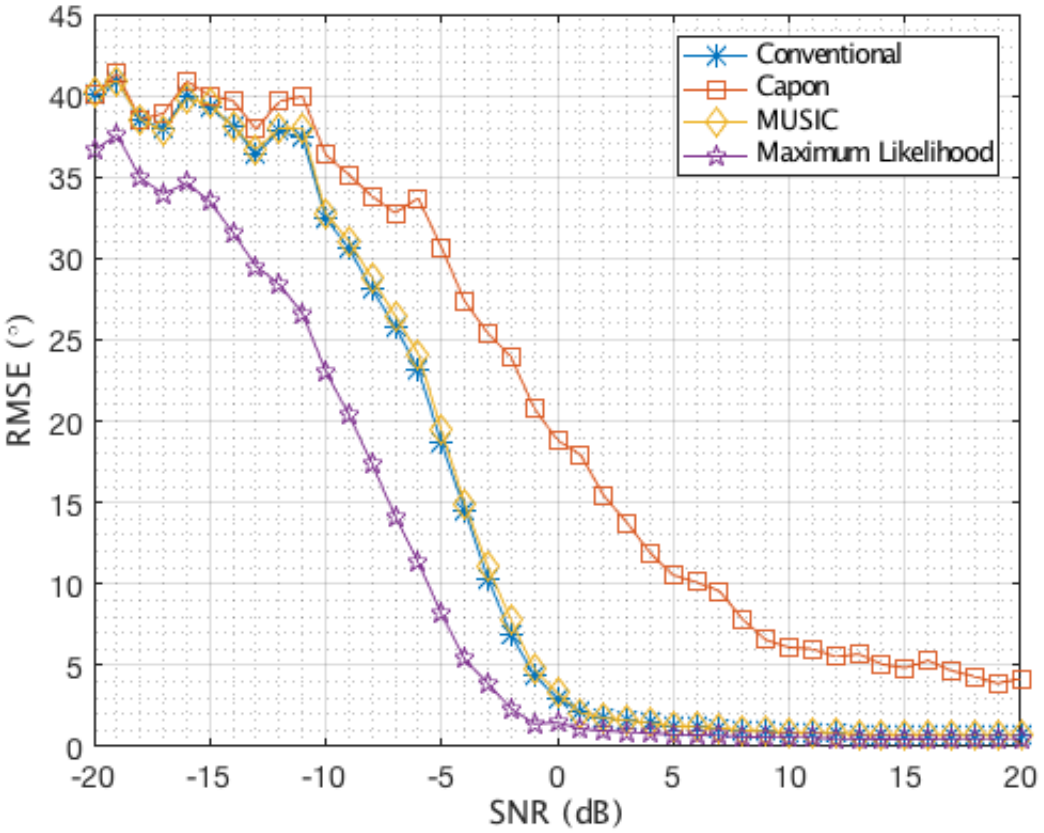

Figure 2.8 – RMSE of Conventional, Capon, MUSIC and Maximum Likelihood angle estimators with $K = 5$, $L = 1$, $M = 4$, Q=181 ($\Delta_\psi = 1.0°$), and $\sigma_f = 1$

Fig. 2.8 and Fig. 2.9 show that the greater the SNR the better the performance of all the techniques. It is evident -as expected- that Maximum Likelihood method gives

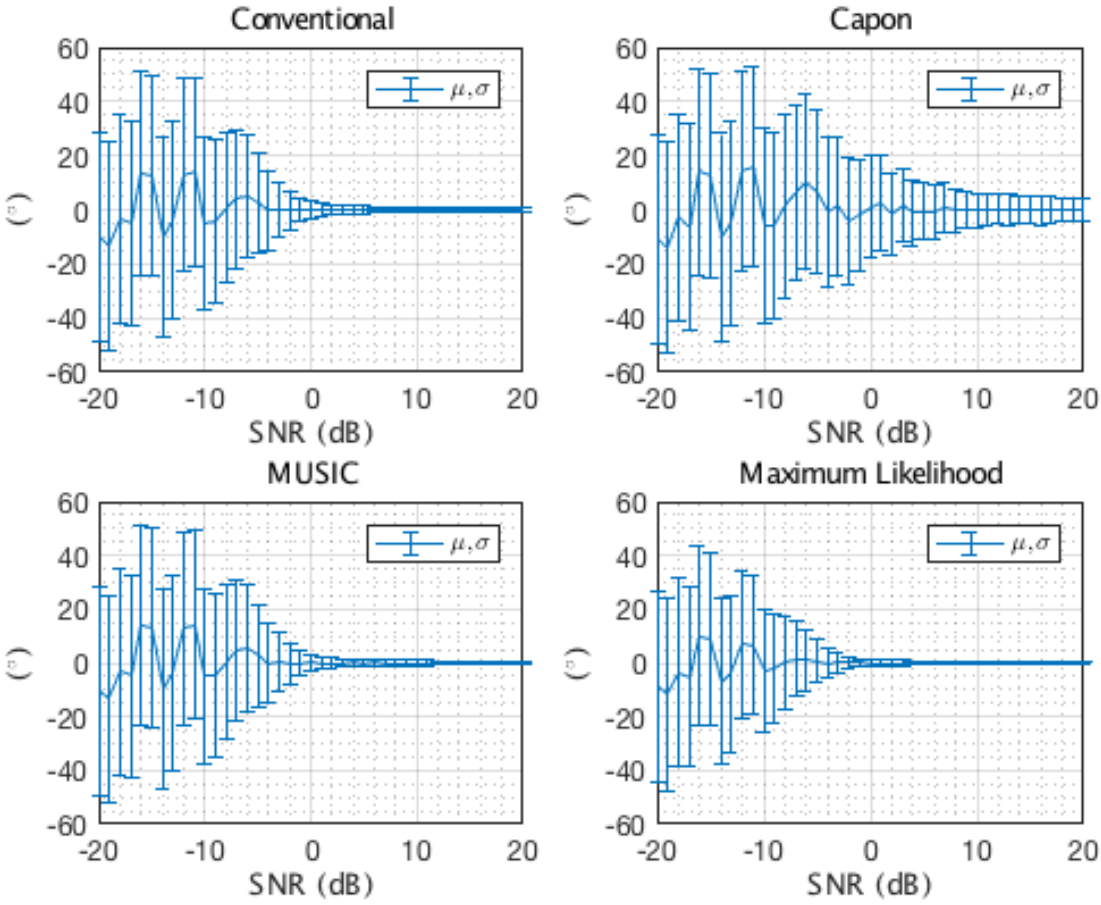

Figure 2.9 – Normalized Mean and Standard Deviation for estimated angle $\hat{\theta}$ of Conventional, Capon, MUSIC and Maximum Likelihood angle estimators with $K = 5$, $L = 1$, $M = 4$, Q=181 ($\Delta_\psi = 1.0°$), and $\sigma_f = 1$

the best performance: it has a smaller error, it tends to the normalized mean faster than the other methods, and its standard deviation is smaller for all the SNR range. On the other hand, the beamforming estimators have a similar performance in all the metrics, with Capon under-performing the other two.

3 Conventional Beamforming Equivalent Random Variable

This chapter shows the derivation of the random variables for conventional beamforming, which their associated PDFs and CDFs are inputs to determine the probability of detection as given in Chapter 5.

3.1 ULA Case

3.1.1 Derivation of the Equivalent Random Variable

Note that (2.11), evaluated for a fixed angle, is a random variable and is defined as:

$$H_{ULA}(\psi) = \frac{\mathbf{a}(\psi)\mathbf{R}\mathbf{a}^H(\psi)}{\mathbf{a}(\psi)\mathbf{a}^H(\psi)} = \frac{\mathbf{a}(\psi)\mathbf{R}\mathbf{a}^H(\psi)}{M}. \tag{3.1}$$

For notation simplicity, we assume $\mathbf{a}(\psi) = \mathbf{a}_\psi$ and therefore, the power spectrum, given in (3.1), can be written as:

$$H_{ULA} = \frac{\mathbf{a}_\psi \mathbf{R}\mathbf{a}_\psi^H}{M}. \tag{3.2}$$

which its reduction/simplification and its associated PDFs and CDFs are our objective. We start by redefining $\mathbf{r}_k$ (2.2):

$$\mathbf{r}_k = \mathbf{a}_\theta \circ \mathbf{h}_k s(t) + \mathbf{n}_k, \tag{3.3}$$

where r_{ki} is the i-th element of $\mathbf{r}_k$, and a_{θ_i} is the i-th element of $\mathbf{a}_\theta$. We continue by deriving the mean and variance of $\mathbf{r}_k$. Since the sum of complex Gaussian random variables is also Gaussian distributed, the real and imaginary part of r_{ki} are distributed as:

$$\Re(r_{ki}) \sim N\left(\frac{L}{\sqrt{2}}\left(\Re(a_{\theta_i}) - \Im(a_{\theta_i})\right), \frac{\sigma_n^2 + \sigma_f^2}{2}\right), \tag{3.4}$$

$$\Im(r_{ki}) \sim N\left(\frac{L}{\sqrt{2}}\left(\Re(a_{\theta_i}) + \Im(a_{\theta_i})\right), \frac{\sigma_n^2 + \sigma_f^2}{2}\right), \tag{3.5}$$

$$\Re(r_{ki}) \sim N\left(\frac{L}{\sqrt{2}}\left(\cos\left(i\frac{2\pi\Delta}{\lambda}\sin(\theta)\right) - \sin\left(i\frac{2\pi\Delta}{\lambda}\sin(\theta)\right)\right), \frac{\sigma_n^2 + \sigma_f^2}{2}\right), \tag{3.6}$$

$$\Im(r_{ki}) \sim N\left(\frac{L}{\sqrt{2}}\left(\cos\left(i\frac{2\pi\Delta}{\lambda}\sin(\theta)\right) + \sin\left(i\frac{2\pi\Delta}{\lambda}\sin(\theta)\right)\right), \frac{\sigma_n^2 + \sigma_f^2}{2}\right), \tag{3.7}$$

where the notation $N(\mu, \sigma^2)$ stands for a normal distribution with mean μ and variance σ^2.

Expanding (2.10) inside (3.2), we get:

$$H_{ULA} = \frac{1}{KM} \sum_{k=0}^{K-1} \mathbf{a}_\psi \mathbf{r}_k^H \mathbf{r}_k \mathbf{a}_\psi^H. \tag{3.8}$$

Now, we can define the variable $\mathbf{q}_k$ as:

$$\mathbf{q}_k = \mathbf{a}_\psi \mathbf{r}_k^H = \Re(\mathbf{q}_k) + j\Im(\mathbf{q}_k). \tag{3.9}$$

Therefore

$$\mathbf{a}_\psi \mathbf{r}_k^H \mathbf{r}_k \mathbf{a}_\psi^H = \Re(\mathbf{q}_k)^2 + \Im(\mathbf{q}_k)^2, \tag{3.10}$$

which can be expanded as:

$$\mathbf{a}_\psi \mathbf{r}_k^H \mathbf{r}_k \mathbf{a}_\psi^H = \left(\sum_{i=0}^{M-1} \Re(a_{\psi_i})\Re(r_{ki}) + \Im(a_{\psi_i})\Im(r_{ki}) \right)^2 + \left(\sum_{i=0}^{M-1} -\Re(a_{\psi_i})\Im(r_{ki}) + \Im(a_{\psi_i})\Re(r_{ki}) \right)^2, \tag{3.11}$$

$$\begin{aligned} \mathbf{a}_\psi \mathbf{r}_k^H \mathbf{r}_k \mathbf{a}_\psi^H = &\left(\sum_{i=0}^{M-1} \cos\left(i\frac{2\pi\Delta}{\lambda} \sin(\psi) \right) \Re(r_{ki}) + \sin\left(i\frac{2\pi\Delta}{\lambda} \sin(\psi) \right) \Im(r_{ki}) \right)^2 \\ &+ \left(\sum_{i=0}^{M-1} -\cos\left(i\frac{2\pi\Delta}{\lambda} \sin(\psi) \right) \Im(r_{ki}) + \sin\left(i\frac{2\pi\Delta}{\lambda} \sin(\psi) \right) \Re(r_{ki}) \right)^2. \end{aligned} \tag{3.12}$$

Note that all the terms inside the summation are Gaussian distributed since r_{ki} is Gaussian and a_{ψ_i} is a constant. Also, the real and imaginary part of r_{ki} are independent. Now defining the new Gaussian variables as:

$$u_{ki} = \Re(a_{\psi_i})\Re(r_{ki}) = \cos\left(i\frac{2\pi\Delta}{\lambda} \sin(\psi) \right) \Re(r_{ki}), \tag{3.13}$$

$$\delta_{ki} = \Im(a_{\psi_i})\Im(r_{ki}) = \sin\left(i\frac{2\pi\Delta}{\lambda} \sin(\psi) \right) \Im(r_{ki}), \tag{3.14}$$

$$\eta_{ki} = \Im(a_{\psi_i})\Re(r_{ki}) = \sin\left(i\frac{2\pi\Delta}{\lambda} \sin(\psi) \right) \Re(r_{ki}), \tag{3.15}$$

$$\zeta_{ki} = \Re(a_{\psi_i})\Im(r_{ki}) = \cos\left(i\frac{2\pi\Delta}{\lambda} \sin(\psi) \right) \Im(r_{ki}), \tag{3.16}$$

which are distributed as:

$$u_{ki} \sim N\left(\frac{L \cdot \Re(a_{\psi_i})}{\sqrt{2}} \left(\Re(a_{\theta_i}) - \Im(a_{\theta_i}) \right), \frac{\Re(a_{\psi_i})^2 \cdot \left(\sigma_n^2 + \sigma_f^2 \right)}{2} \right), \tag{3.17}$$

$$\delta_{ki} \sim N\left(\frac{L \cdot \Im(a_{\psi_i})}{\sqrt{2}} \left(\Re(a_{\theta_i}) + \Im(a_{\theta_i}) \right), \frac{\Im(a_{\psi_i})^2 \cdot \left(\sigma_n^2 + \sigma_f^2 \right)}{2} \right), \tag{3.18}$$

$$\eta_{ki} \sim N\left(\frac{L \cdot \Im(a_{\psi_i})}{\sqrt{2}} \left(\Re(a_{\theta_i}) - \Im(a_{\theta_i}) \right), \frac{\Im(a_{\psi_i})^2 \cdot \left(\sigma_n^2 + \sigma_f^2 \right)}{2} \right), \tag{3.19}$$

$$\zeta_{ki} \sim N\left(\frac{L \cdot \Re(a_{\psi_i})}{\sqrt{2}} \left(\Re(a_{\theta_i}) + \Im(a_{\theta_i}) \right), \frac{\Re(a_{\psi_i})^2 \cdot \left(\sigma_n^2 + \sigma_f^2 \right)}{2} \right), \tag{3.20}$$

equivalently:

$$u_{ki} \sim N\left(\frac{L\cdot\cos\left(i\frac{2\pi\Delta}{\lambda}\sin(\psi)\right)}{\sqrt{2}}\left(\cos\left(i\frac{2\pi\Delta}{\lambda}\sin(\theta)\right)-\sin\left(i\frac{2\pi\Delta}{\lambda}\sin(\theta)\right)\right),\frac{\cos^2\left(i\frac{2\pi\Delta}{\lambda}\sin(\psi)\right)\cdot\left(\sigma_n^2+\sigma_f^2\right)}{2}\right) \quad (3.21)$$

$$\delta_{ki} \sim N\left(\frac{L\cdot\sin\left(i\frac{2\pi\Delta}{\lambda}\sin(\psi)\right)}{\sqrt{2}}\left(\cos\left(i\frac{2\pi\Delta}{\lambda}\sin(\theta)\right)+\sin\left(i\frac{2\pi\Delta}{\lambda}\sin(\theta)\right)\right),\frac{\sin^2\left(i\frac{2\pi\Delta}{\lambda}\sin(\psi)\right)\cdot\left(\sigma_n^2+\sigma_f^2\right)}{2}\right) \quad (3.22)$$

$$\eta_{ki} \sim N\left(\frac{L\cdot\sin\left(i\frac{2\pi\Delta}{\lambda}\sin(\psi)\right)}{\sqrt{2}}\left(\cos\left(i\frac{2\pi\Delta}{\lambda}\sin(\theta)\right)-\sin\left(i\frac{2\pi\Delta}{\lambda}\sin(\theta)\right)\right),\frac{\sin^2\left(i\frac{2\pi\Delta}{\lambda}\sin(\psi)\right)\cdot\left(\sigma_n^2+\sigma_f^2\right)}{2}\right) \quad (3.23)$$

$$\zeta_{ki} \sim N\left(\frac{L\cdot\cos\left(i\frac{2\pi\Delta}{\lambda}\sin(\psi)\right)}{\sqrt{2}}\left(\cos\left(i\frac{2\pi\Delta}{\lambda}\sin(\theta)\right)+\sin\left(i\frac{2\pi\Delta}{\lambda}\sin(\theta)\right)\right),\frac{\cos^2\left(i\frac{2\pi\Delta}{\lambda}\sin(\psi)\right)\cdot\left(\sigma_n^2+\sigma_f^2\right)}{2}\right) \quad (3.24)$$

then we can write (3.10) as:

$$\mathbf{a}_\psi\mathbf{r}_k^H\mathbf{r}_k\mathbf{a}_\psi^H=\left(\sum_{i=0}^{M-1}u_{ki}+\delta_{ki}\right)^2+\left(\sum_{i=0}^{M-1}\eta_{ki}-\zeta_{ki}\right)^2. \quad (3.25)$$

The terms inside the sums are also Gaussian distributed and recalling that $\Re(a_{\psi_i})^2+\Im(a_{\psi_i})^2=1$, we have that:

$$\rho_{ki} \sim N\left(\frac{L}{\sqrt{2}}\cdot\left(\Re(a_{\psi_i})\left(\Re(a_{\theta_i})-\Im(a_{\theta_i})\right)+\Im(a_{\psi_i})\left(\Re(a_{\theta_i})+\Im(a_{\theta_i})\right)\right),\frac{\sigma_n^2+\sigma_f^2}{2}\right), \quad (3.26)$$

$$\tau_{ki} \sim N\left(\frac{L}{\sqrt{2}}\cdot\left(\Im(a_{\psi_i})\left(\Re(a_{\theta_i})-\Im(a_{\theta_i})\right)-\Re(a_{\psi_i})\left(\Re(a_{\theta_i})+\Im(a_{\theta_i})\right)\right),\frac{\sigma_n^2+\sigma_f^2}{2}\right). \quad (3.27)$$

By trigonometrical reduction:

$$\Re(a_{\psi_i})\left(\Re(a_{\theta_i})-\Im(a_{\theta_i})\right)+\Im(a_{\psi_i})\left(\Re(a_{\theta_i})+\Im(a_{\theta_i})\right)=\cos\left(i\frac{2\pi\Delta}{\lambda}\Xi\right)+\sin\left(i\frac{2\pi\Delta}{\lambda}\Xi\right), \quad (3.28)$$

$$\Im(a_{\psi_i})\left(\Re(a_{\theta_i})-\Im(a_{\theta_i})\right)-\Re(a_{\psi_i})\left(\Re(a_{\theta_i})+\Im(a_{\theta_i})\right)=\sin\left(i\frac{2\pi\Delta}{\lambda}\Xi\right)-\cos\left(i\frac{2\pi\Delta}{\lambda}\Xi\right), \quad (3.29)$$

where

$$\Xi=\sin(\psi)-\sin(\theta). \quad (3.30)$$

Therefore equations (3.26) and (3.27) can be rewritten as:

$$\rho_{ki} \sim N\left(\frac{L}{\sqrt{2}}\cdot\left(\cos\left(i\frac{2\pi\Delta}{\lambda}\Xi\right)+\sin\left(i\frac{2\pi\Delta}{\lambda}\Xi\right)\right),\frac{\sigma_n^2+\sigma_f^2}{2}\right), \quad (3.31)$$

$$\tau_{ki} \sim N\left(\frac{L}{\sqrt{2}}\cdot\left(\sin\left(i\frac{2\pi\Delta}{\lambda}\Xi\right)-\cos\left(i\frac{2\pi\Delta}{\lambda}\Xi\right)\right),\frac{\sigma_n^2+\sigma_f^2}{2}\right). \quad (3.32)$$

so we write (3.25) as:

$$\mathbf{a}_\psi\mathbf{r}_k^H\mathbf{r}_k\mathbf{a}_\psi^H=\left(\sum_{i=0}^{M-1}\rho_{ki}\right)^2+\left(\sum_{i=0}^{M-1}\tau_{ki}\right)^2 \quad (3.33)$$

Once again due to independence of ρ_{ki} and τ_{ki}, the sum of M Gaussian variables is another Gaussian variable with mean equal to the sum of the M means and variance equal to the sum of the M variances, therefore we have:

$$\epsilon_k = \sum_{i=0}^{M-1} \rho_{ki}, \tag{3.34}$$

$$\omega_k = \sum_{i=0}^{M-1} \tau_{ki}, \tag{3.35}$$

which are distributed as:

$$\epsilon_k \sim N\left(\frac{L}{\sqrt{2}} \cdot \left(\sum_{i=0}^{M-1} \cos\left(i\frac{2\pi\Delta}{\lambda}\Xi\right) + \sin\left(i\frac{2\pi\Delta}{\lambda}\Xi\right)\right), \frac{M \cdot (\sigma_n^2 + \sigma_f^2)}{2}\right), \tag{3.36}$$

$$\omega_k \sim N\left(\frac{L}{\sqrt{2}} \cdot \left(\sum_{i=0}^{M-1} \sin\left(i\frac{2\pi\Delta}{\lambda}\Xi\right) - \cos\left(i\frac{2\pi\Delta}{\lambda}\Xi\right)\right), \frac{M \cdot (\sigma_n^2 + \sigma_f^2)}{2}\right), \tag{3.37}$$

then we can write (3.8) as:

$$H_{ULA} = \frac{1}{KM} \sum_{k=0}^{K-1} \epsilon_k^2 + \omega_k^2. \tag{3.38}$$

Since the sum of independent non-central square Gaussians with $\sigma^2 = 1$ is a non-central *Chi*-squared distributed random variable, we get that (3.38) (after unitary variance normalization) can be written as:

$$H_{ULA} = \frac{\sigma_n^2 + \sigma_f^2}{2K} \cdot (\iota + \nu), \tag{3.39}$$

where

$$\iota \sim \chi_{nc}^2\left(K, \frac{KL^2}{M\left(\sigma_n^2 + \sigma_f^2\right)}\left(\sum_{i=0}^{M-1} \cos\left(i\frac{2\pi\Delta}{\lambda}\Xi\right) + \sin\left(i\frac{2\pi\Delta}{\lambda}\Xi\right)\right)^2\right), \tag{3.40}$$

$$\nu \sim \chi_{nc}^2\left(K, \frac{KL^2}{M\left(\sigma_n^2 + \sigma_f^2\right)}\left(\sum_{i=0}^{M-1} \sin\left(i\frac{2\pi\Delta}{\lambda}\Xi\right) - \cos\left(i\frac{2\pi\Delta}{\lambda}\Xi\right)\right)^2\right), \tag{3.41}$$

and $\chi_{nc}^2(\kappa, \lambda)$ is the non-central *Chi*-squared (PAPOULIS; PILLAI, 2002) distribution with the parameters $\kappa > 0$ (degrees of freedom) and $\lambda > 0$ (non-centrality).

Finally, by non-central *Chi*-squared addition properties we get that

$$H_{ULA} = \frac{\sigma_n^2 + \sigma_f^2}{2K} \Omega_{(\psi,\theta)}, \tag{3.42}$$

where

$$\Omega_{(\psi,\theta)} \sim \chi_{nc}^2\left(2K, \frac{KL^2\left(\pi_{1_{(\psi,\theta)}}^2 + \pi_{2_{(\psi,\theta)}}^2\right)}{M\left(\sigma_n^2 + \sigma_f^2\right)}\right), \tag{3.43}$$

and

$$\pi_{1_{(\psi,\theta)}} = \sum_{i=0}^{M-1} \left(\cos\left(i\frac{2\pi\Delta}{\lambda}\Xi \right) + \sin\left(i\frac{2\pi\Delta}{\lambda}\Xi \right) \right), \tag{3.44}$$

$$\pi_{2_{(\psi,\theta)}} = \sum_{i=0}^{M-1} \left(\sin\left(i\frac{2\pi\Delta}{\lambda}\Xi \right) - \cos\left(i\frac{2\pi\Delta}{\lambda}\Xi \right) \right). \tag{3.45}$$

Therefore, H_{ULA} is a scaled non-central *Chi*-squared distributed random variable. This result shows that the spatial power spectrum given in (2.11) could be seen as an equivalent random variable, which depends on the spatial frequency associated to the angle ψ (i.e. each one of the Q steering discretized angles of the span), θ (i.e the AoA), besides the environment and controllable variables (the number of antennas M, the number of snapshots K, the fading mean component (LoS) L, the fading variance σ_f^2 and the noise variance σ_n^2).

3.1.2 PDF and CDF

The derived PDF for H_{ULA} (using the characteristic PDF for scaled non-central *Chi* squared distribution) is given as:

$$f_{H_{ULA}}(x) = \frac{K}{\sigma_n^2+\sigma_f^2} e^{-\frac{K\left(2Mx+\left(\pi_{1_{(\psi,\theta)}}^2+\pi_{2_{(\psi,\theta)}}^2\right)L^2\right)}{2M(\sigma_n^2+\sigma_f^2)}} \left(\frac{2Mx}{\left(\pi_{1_{(\psi,\theta)}}^2+\pi_{2_{(\psi,\theta)}}^2\right)L^2} \right)^{\frac{K-1}{2}} \cdot I_{K-1}\left(\frac{KL}{\sigma_n^2+\sigma_f^2}\sqrt{\frac{2\left(\pi_{1_{(\psi,\theta)}}^2+\pi_{2_{(\psi,\theta)}}^2\right)x}{M}} \right), \tag{3.46}$$

where $I_c(d)$ is the modified Bessel function of the first kind with parameters $c \geq 0$ and $d \geq 0$. The corresponding CDF (using the characteristic CDF for scaled non-central *Chi* squared distribution) can be found as:

$$F_{H_{ULA}}(x) = 1 - Q_K\left(\sqrt{\frac{K\left(\pi_{1_{(\psi,\theta)}}^2+\pi_{2_{(\psi,\theta)}}^2\right)L^2}{M\left(\sigma_n^2+\sigma_f^2\right)}}, \sqrt{\frac{2K}{\sigma_n^2+\sigma_f^2}\,x} \right), \tag{3.47}$$

where $Q_e(a,b)$ is the Marcum-Q function with parameters $a \geq 0$, $b \geq 0$ and $e \geq 0$.

3.1.3 Mean and Variance

The mean of the random variable H_{ULA} (using the characteristic mean for scaled non-central *Chi* squared distribution) can be calculated as:

$$\mathbf{E}[H_{ULA}] = \frac{2M\left(\sigma_n^2+\sigma_f^2\right)+L^2\left(\pi_{1_{(\psi,\theta)}}^2+\pi_{2_{(\psi,\theta)}}^2\right)}{2M}, \tag{3.48}$$

and the variance (using the characteristic variance for scaled non-central *Chi* squared distribution) is given as:

$$\mathbf{var}[H_{ULA}] = \frac{M\left(\sigma_n^2 + \sigma_f^2\right)^2 + (\sigma_n^2 + \sigma_f^2)L^2\left(\pi^2_{1_{(\psi,\theta)}} + \pi^2_{2_{(\psi,\theta)}}\right)}{KM}. \tag{3.49}$$

Based on these analytical equations, it is evident that the mean does not depend on the number of snapshots K, and it is strongly dependent on the product of the number of antennas and the fading mean component. On the other hand, the variance is highly sensitive to the noise and fading variance. These could be mitigated by increasing the parameter K, which will reduce the variance.

3.1.3.1 Influence of parameters ψ and θ

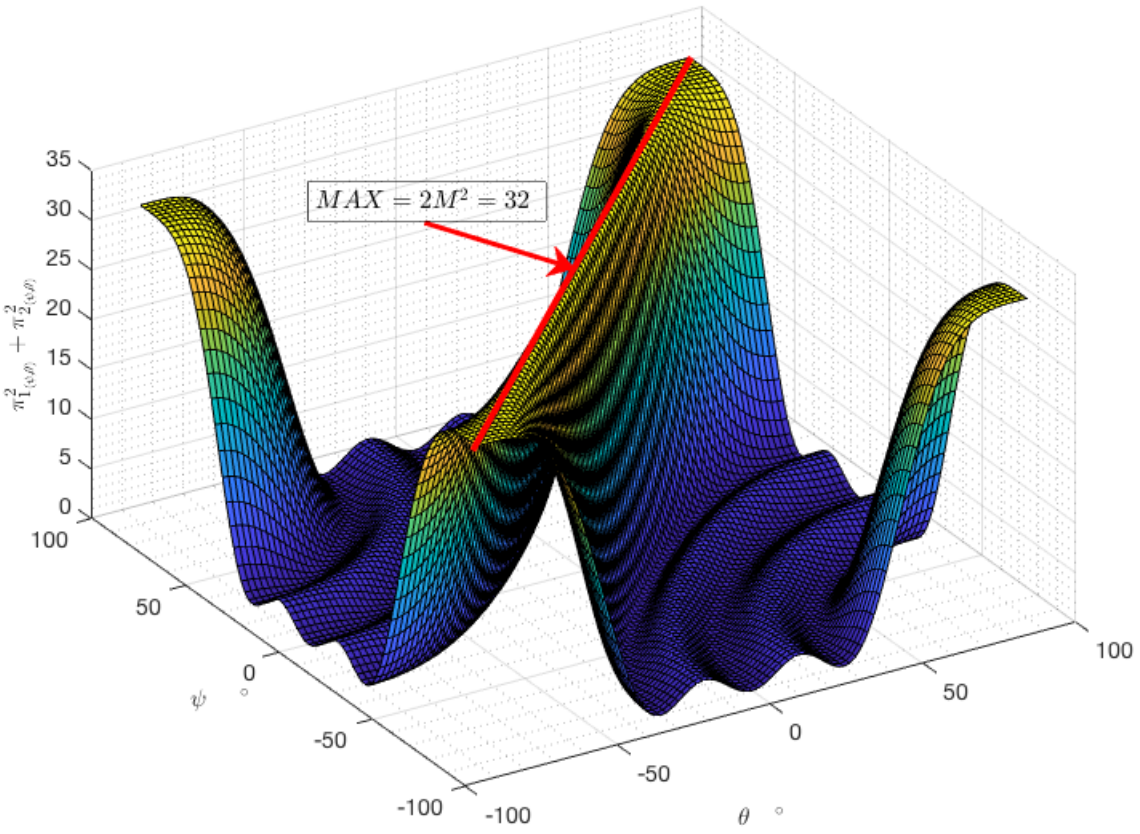

Figure 3.1 – $\pi^2_{1_{(\psi,\theta)}} + \pi^2_{2_{(\psi,\theta)}}$ versus (ψ, θ) for H_{ULA} with $M = 4$.

Due to the linear dependence of the mean and variance on $\pi^2_{1_{(\psi,\theta)}} + \pi^2_{2_{(\psi,\theta)}}$ ((3.48) and (3.49)), Fig. 3.1 reflects the influence of steering angles (ψ, θ) on H_{ULA} mean and variance. It is evident that $\pi^2_{1_{(\psi,\theta)}} + \pi^2_{2_{(\psi,\theta)}}$ gets its maximum ($\pi^2_{1_{(\psi,\theta)}} + \pi^2_{2_{(\psi,\theta)\,MAX}} = 2M^2$) when $\psi = \theta$ and also when the difference between $\{\psi, \theta\}$ is the biggest possible. This fact

shows that the conventional beamforming, besides the influence of all the environment (L, σ_n, σ_f) and controllable parameters (M, K) is directly affected by the AoA itself. Particularly, variance models the power of the signal. Therefore for the H_{ULA} case, a greater value implies more power associated with the AoA. This occurrence confirms the principle of the conventional beamforming approach: to find the maximum power associated with the Q possible steering angles of the spatial power spectrum. Finally, the maximum in the extremes of the $\{\psi, \theta\}$ difference shows that this situation shall be avoided, in other words, the steering shall be done in a range that reduces the effect of the $\psi \neq \theta$ circumstance, like $\{-\frac{\pi}{3}, \frac{\pi}{3}\}$.

3.1.4 Equivalent Random Variable for AoA

Our primary objective focuses the research on finding the equivalent random variable when $\psi = \theta$, as established in the following rationale. We define:

$$H_{ULA}(\psi = \theta) = P_{ULA}, \tag{3.50}$$

therefore

$$P_{ULA} = \frac{\sigma_n^2 + \sigma_f^2}{2K} \Omega_{(\theta,\theta)}, \tag{3.51}$$

where

$$\Omega_{(\theta,\theta)} \sim \chi^2_{nc} \left(2K, \frac{KL^2 \left(\pi^2_{1_{(\theta,\theta)}} + \pi^2_{2_{(\theta,\theta)}} \right)}{M \left(\sigma_n^2 + \sigma_f^2 \right)} \right). \tag{3.52}$$

Here

$$\Xi = \sin(\psi) - \sin(\psi) = 0 \tag{3.53}$$

Therefore π_1 and π_2 change into:

$$\pi_1 = \sum_{i=0}^{M-1} \cos\left(i \frac{2\pi\Delta}{\lambda} 0 \right) + \sin\left(i \frac{2\pi\Delta}{\lambda} 0 \right) = \sum_{i=0}^{M-1} \cos(0) + \sin(0) = \sum_{i=0}^{M-1} 1 = M \tag{3.54}$$

$$\pi_2 = \sum_{i=0}^{M-1} \sin\left(i \frac{2\pi\Delta}{\lambda} 0 \right) - \cos\left(i \frac{2\pi\Delta}{\lambda} 0 \right) = \sum_{i=0}^{M-1} \sin(0) - \cos(0) = \sum_{i=0}^{M-1} -1 = -M \tag{3.55}$$

$$\pi^2_{1_{(\theta,\theta)}} + \pi^2_{2_{(\psi,\theta)}} = (M^2) + (-M)^2 = 2M^2, \tag{3.56}$$

turning (3.52) into:

$$\Omega_{(\theta,\theta)} \sim \chi^2_{nc} \left(2K, \frac{2KML^2}{\sigma_n^2 + \sigma_f^2} \right). \tag{3.57}$$

Correspondingly, the PDF, CDF, $\mathbf{E}[.]$ and $\mathbf{var}[.]$ acquire their own values:

$$f_{P_{ULA}}(x) = \frac{K}{\sigma_n^2 + \sigma_f^2} e^{-\frac{K\left(x + ML^2\right)}{\sigma_n^2 + \sigma_f^2}} \left(\frac{x}{ML^2} \right)^{\frac{K-1}{2}} I_{K-1} \left(\frac{2KL}{\sigma_n^2 + \sigma_f^2} \sqrt{Mx} \right), \tag{3.58}$$

$$F_{P_{ULA}}(x) = 1 - Q_K\left(\sqrt{\frac{2KML^2}{\sigma_n^2+\sigma_f^2}}, \sqrt{\frac{2K}{\sigma_n^2+\sigma_f^2}\,x}\right), \tag{3.59}$$

$$\mathbf{E}[P_{ULA}] = \sigma_n^2 + \sigma_f^2 + ML^2, \tag{3.60}$$

$$\mathbf{var}[P_{ULA}] = \frac{\left(\sigma_n^2+\sigma_f^2\right)^2 + (\sigma_n^2+\sigma_f^2)2ML^2}{K}. \tag{3.61}$$

As in the general case, mean does not depend on the number of snapshots K and variance is sensitive to the noise and the fading variances. Finally, there is no dependence on ψ neither θ angle.

3.1.5 Particular Cases for P_{ULA}

3.1.5.1 Absence of Rayleigh Fading

When the fading is not present in the model, $\sigma_f^2 = 0$ and $L = 1$. In this case, the performance is very similar to the general case, but now the parameters M and K have more influence on the PDF. Consequently, the detection is more controllable.

3.1.5.2 Absence of fading mean (Null LoS)

When the fading mean is not present in the model (i.e. there is no LoS component), $L = 0$. In this case the P_{ULA} will be given as:

$$P_{ULA} = \frac{\sigma_n^2+\sigma_f^2}{2K}\Omega_{(\theta,\theta)}, \tag{3.62}$$

where

$$\Omega_{(\theta,\theta)} \sim \chi^2_{nc}\left(2K, \frac{2KM0^2}{\sigma_n^2+\sigma_f^2}\right). \tag{3.63}$$

$$\Omega_{(\theta,\theta)} \sim \chi^2_{nc}\left(2K, 0\right). \tag{3.64}$$

Note that a null non centrality parameter for a non-central *Chi* squared random variable implies that $\Omega_{(\theta,\theta)}$ is distributed as a central *Chi*-squared distribution, or in other words, a *Chi*-squared distribution with parameter $\kappa = 2K$ (degrees of freedom).
The mean of the random variable (using the characteristic mean for scaled central *Chi* squared distribution) can be calculated as:

$$\mathbf{E}[P_{ULA}] = \sigma_n^2 + \sigma_f^2, \tag{3.65}$$

and the variance (using the characteristic variance for scaled central *Chi* squared distribution) is given as:

$$\mathbf{var}[P_{ULA}] = \frac{\left(\sigma_n^2+\sigma_f^2\right)^2}{K}. \tag{3.66}$$

After replacing $L = 0$ in (3.58) and reducing the Bessel function, the PDF is given as:

$$f_{H_{ULA}}(x) = \left(\frac{K}{\sigma_n^2 + \sigma_f^2}\right)^K \frac{x^{K-1} e^{-\frac{xK}{\sigma_n^2+\sigma_f^2}}}{\Gamma(K)}. \tag{3.67}$$

In the same fashion for (3.59) and reducing the Marcum-Q function, the CDF is given as:

$$F_{P_{ULA}}(x) = 1 - \frac{\gamma\left(K, \frac{Kx}{\sigma_n^2+\sigma_f^2}\right)}{\Gamma(K)}, \tag{3.68}$$

where $\gamma(\cdot,\cdot)$ is the incomplete Gamma function, and $\Gamma(\cdot)$ is the gamma function.
These derivations show that the absence of the fading mean eliminates the influence of the array (parameter M absent), therefore K is the only variable available to improve the detection. The AoA estimation detection now strongly depends on the specific characteristics of the fading (multipath propagation, signal reflection, signal diffraction) and the noise which can result in a mediocre performance for angle appraisal.

3.2 URA Case

3.2.1 Derivation of the Equivalent Random Variable

Note that (2.13), evaluated for a fixed angle is a random variable defined as:

$$H_{URA}(\psi,\xi) = \frac{\mathbf{a}(\psi,\xi)\mathbf{R}\mathbf{a}^H(\psi,\xi)}{\mathbf{a}(\psi,\xi)\mathbf{a}^H(\psi,\xi)}. \tag{3.69}$$

Recalling subsection 2.1.1, the $\mathbf{r}_k$ signal vector size is $1 \times M_x M_y$ and $\mathbf{a}(\psi,\xi) = \mathbf{a}_{(\psi,\xi)}$, therefore the power spectrum, given in (3.69), can be written as:

$$H_{URA} = \frac{\mathbf{a}_{(\psi,\xi)}\mathbf{R}\mathbf{a}^H_{(\psi,\xi)}}{M_x M_y} \tag{3.70}$$

The next steps are the same as in the ULA case, resulting on

$$H_{URA} = \frac{\sigma_n^2 + \sigma_f^2}{2K}\Omega_{(\psi,\theta,\xi,\phi)}, \tag{3.71}$$

where

$$\Omega_{(\psi,\theta,\xi,\phi)} \sim \chi^2_{nc}\left(2K, \frac{KL^2\left(\pi^2_{1_{(\psi,\theta,\xi,\phi)}} + \pi^2_{2_{(\psi,\theta,\xi,\phi)}}\right)}{M_x M_y\left(\sigma_n^2 + \sigma_f^2\right)}\right), \tag{3.72}$$

$$\pi_{1_{(\psi,\theta,\xi,\phi)}} = \sum_{i=0}^{M_x M_y - 1}\left(\Re(a_{(\psi,\xi)_i})\left(\Re(a_{(\theta,\phi)_i}) - \Im(a_{(\theta,\phi)_i})\right) + \Im(a_{(\psi,\xi)_i})\left(\Re(a_{(\theta,\phi)_i}) + \Im(a_{(\theta,\phi)_i})\right)\right) \tag{3.73}$$

$$\pi_{2_{(\psi,\theta,\xi,\phi)}} = \sum_{i=0}^{M_x M_y - 1} \left(\Im(a_{(\psi,\xi)_i}) \left(\Re(a_{(\theta,\phi)_i}) - \Im(a_{(\theta,\phi)_i}) \right) - \Re(a_{(\psi,\xi)_i}) \left(\Re(a_{(\theta,\phi)_i}) + \Im(a_{(\theta,\phi)_i}) \right) \right) \tag{3.74}$$

Therefore, H_{URA} is a scaled non-central *Chi*-squared distributed random variable. $\chi^2_{nc}(\kappa, \lambda)$ is the non-central *Chi*-squared (PAPOULIS; PILLAI, 2002) distribution with the parameters $\kappa > 0$ (degrees of freedom) and $\lambda > 0$ (non-centrality).

3.2.2 PDF and CDF

The derived PDF for H_{URA} (using the characteristic PDF for scaled non-central *Chi* squared distribution) is given as:

$$f_{H_{URA}}(x) = \frac{K}{\sigma_n^2 + \sigma_f^2} e^{-\frac{K\left(2M_x M_y x + \left(\pi^2_{1_{(\psi,\theta,\xi,\phi)}} + \pi^2_{2_{(\psi,\theta,\xi,\phi)}}\right) L^2\right)}{2M_x M_y (\sigma_n^2 + \sigma_f^2)}} \left(\frac{2M_x M_y x}{\left(\pi^2_{1_{(\psi,\theta,\xi,\phi)}} + \pi^2_{2_{(\psi,\theta,\xi,\phi)}}\right) L^2} \right)^{\frac{K-1}{2}} I_{K-1}\left(\frac{KL}{\sigma_n^2 + \sigma_f^2} \sqrt{\frac{2\left(\pi^2_{1_{(\psi,\theta,\xi,\phi)}} + \pi^2_{2_{(\psi,\theta,\xi,\phi)}}\right) x}{M_x M_y}} \right), \tag{3.75}$$

where $I_c(d)$ is the modified Bessel function of the first kind with parameters $c \geq 0$ and $d \geq 0$. The corresponding CDF (using the characteristic CDF for scaled non-central *Chi* squared distribution) can be found as:

$$F_{H_{URA}}(x) = 1 - Q_K\left(\sqrt{\frac{K\left(\pi^2_{1_{(\psi,\theta,\xi,\phi)}} + \pi^2_{2_{(\psi,\theta,\xi,\phi)}}\right) L^2}{M_x M_y \left(\sigma_n^2 + \sigma_f^2\right)}}, \sqrt{\frac{2K}{\sigma_n^2 + \sigma_f^2} x} \right), \tag{3.76}$$

where $Q_e(a, b)$ is the Marcum-Q function with parameters $a \geq 0$, $b \geq 0$ and $e \geq 0$.

3.2.3 Mean and Variance

The mean of the random variable H_{URA} (using the characteristic mean for scaled non-central *Chi* squared distribution) can be calculated as:

$$\mathbf{E}[H_{URA}] = \frac{2M_x M_y \left(\sigma_n^2 + \sigma_f^2\right) + L^2 \left(\pi^2_{1_{(\psi,\theta,\xi,\phi)}} + \pi^2_{2_{(\psi,\theta,\xi,\phi)}}\right)}{2M_x M_y}, \tag{3.77}$$

and the variance (using the characteristic variance for scaled non-central *Chi* squared distribution) is given as:

$$\mathbf{var}[H_{URA}] = \frac{M_x M_y \left(\sigma_n^2 + \sigma_f^2\right)^2 + (\sigma_n^2 + \sigma_f^2) L^2 \left(\pi^2_{1_{(\psi,\theta,\xi,\phi)}} + \pi^2_{2_{(\psi,\theta,\xi,\phi)}}\right)}{K M_x M_y}. \tag{3.78}$$

These equations show that geometry does not have an impact on the equivalent model: all parameters remain the same in both array configurations and the only generalization is the total number of antennas.

3.2.4 Equivalent Random Variable for AoA

In a similar fashion of the ULA case, we can obtain the equivalent random variable for URA when $\psi = \theta$ and $\xi = \phi$, as established in the next equations:

$$H_{URA}(\psi = \theta, \xi = \phi) = P_{URA} = \frac{\sigma_n^2 + \sigma_f^2}{2K} \Omega_{(\theta,\theta,\phi,\phi)}, \tag{3.79}$$

where

$$\Omega_{(\theta,\theta,\phi,\phi)} \sim \chi^2_{nc} \left(2K, \frac{KL^2 \left(\pi^2_{1_{(\theta,\theta,\phi,\phi)}} + \pi^2_{2_{(\theta,\theta,\phi,\phi)}} \right)}{M_x M_y \left(\sigma_n^2 + \sigma_f^2 \right)} \right), \tag{3.80}$$

and after mathematical simplification

$$\pi^2_{1_{(\theta,\theta,\phi,\phi)}} + \pi^2_{2_{(\psi,\theta,\xi,\phi)}} = 2 \left(M_x M_y \right)^2, \tag{3.81}$$

turning (3.80) into:

$$\Omega_{(\theta,\theta,\phi,\phi)} \sim \chi^2_{nc} \left(2K, \frac{2KM_x M_y L^2}{\sigma_n^2 + \sigma_f^2} \right). \tag{3.82}$$

Correspondingly, the PDF, CDF, $\mathbf{E}[.]$ and $\mathbf{var}[.]$ can be written respectively as:

$$f_{P_{URA}}(x) = \frac{K}{\sigma_n^2 + \sigma_f^2} e^{-\frac{K\left(x + M_x M_y L^2\right)}{\sigma_n^2 + \sigma_f^2}} \left(\frac{x}{M_x M_y L^2} \right)^{\frac{K-1}{2}} I_{K-1} \left(\frac{2KL}{\sigma_n^2 + \sigma_f^2} \sqrt{M_x M_y x} \right), \tag{3.83}$$

$$F_{P_{URA}}(x) = 1 - Q_K \left(\sqrt{\frac{2KM_x M_y L^2}{\sigma_n^2 + \sigma_f^2}}, \sqrt{\frac{2K}{\sigma_n^2 + \sigma_f^2}\, x} \right), \tag{3.84}$$

$$\mathbf{E}[P_{URA}] = \sigma_n^2 + \sigma_f^2 + M_x M_y L^2, \tag{3.85}$$

$$\mathbf{var}[P_{URA}] = \frac{\left(\sigma_n^2 + \sigma_f^2 \right)^2 + (\sigma_n^2 + \sigma_f^2) 2M_x M_y L^2}{K}. \tag{3.86}$$

As in the general case, mean does not depend on number of snapshots K and variance is sensitive to noise and fading variances.

3.2.5 Particular Cases for P_{URA}

Analyses of special cases like the absence of Rayleigh fading ($\sigma_f = 0$) and absence of the fading mean ($L = 0$) (i.e. LoS is null) remain the same as in the ULA case. The effect of changing parameter M for $M_x M_y$ does not affect the behavior of derived equations in both cases.

4 Numerical Results: Random Variable Characterization

Chapter 4 characterizes the equivalent random variable presenting numerical simulated and analytical results of the PDFs, CDFs, **E**[.] and **var**[.] for single and multiple RBSs (ULA and URA case) in numerous scenarios, as well as a particular discussion for each case.

4.1 ULA and URA general equivalent random variables

Fig. 4.1 shows the analytical PDF, given in (3.46), and the normalized histogram of the simulated random variable, given in (3.2) for three different steering angles of ULA case. Fig. 4.2 shows the analytical CDF, given in (3.47), and the associated CDF of the simulated random variable, given in (3.2) for three different steering angles of ULA case. As expected, both plots match perfectly, once that our analytical results are exact.

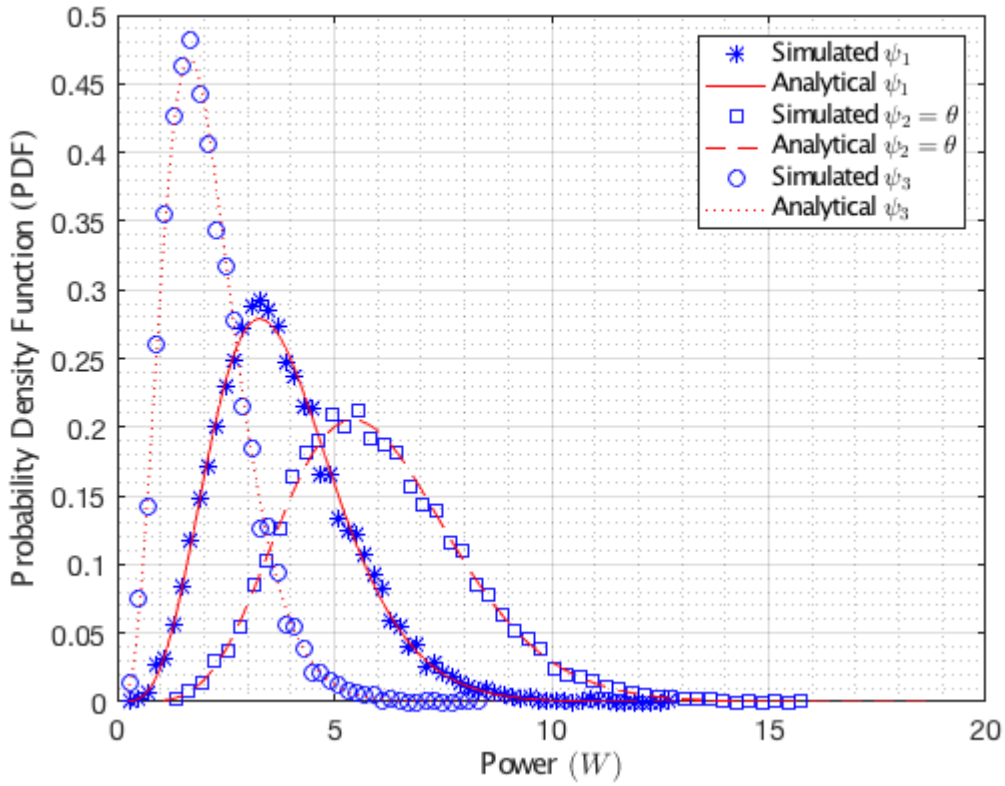

Figure 4.1 – Normalized Histogram for 10^4 realizations of (3.2) and analytical PDF given in (3.46), with $K = 5$, $M = 4$, $L = 1$, $\sigma_f = 1$ and $\sigma_n = 1$ (SNR=0 dB) for $\psi_1 = 15°$, $\psi_2 = \theta = 30°$ $\psi_3 = 70°$ in ULA case.

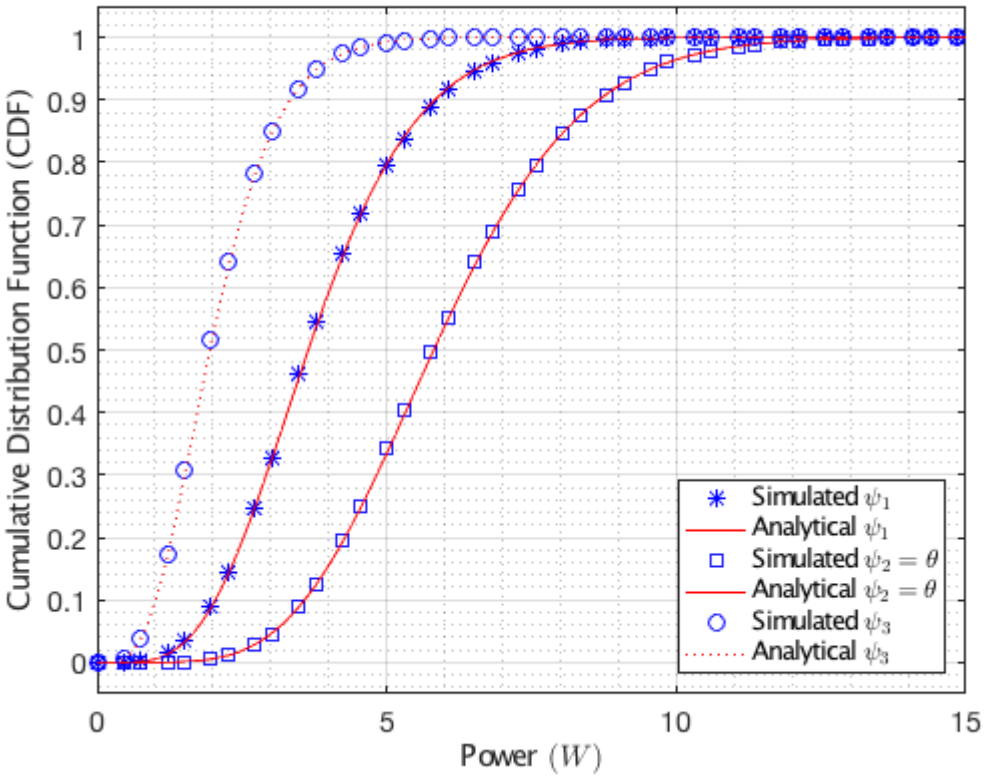

Figure 4.2 – Associated CDF for 10^4 realizations of (3.2) and analytical CDF given in (3.47), with $K = 5$, $M = 4$, $L = 1$, $\sigma_f = 1$ and $\sigma_n = 1$ (SNR=0 dB) for $\psi_1 = 15°$, $\psi_2 = \theta = 30°$ $\psi_3 = 70°$ in ULA case.

Fig. 4.3 and Fig. 4.4 expose the URA case with the same parameters of ULA case, including $M_x = M_y$ that maintains parameter M identical in (3.70), (3.72), (3.75) and (3.76) as stated in section 3.2. Again there is a perfect match.

Fig. 4.2 and Fig. 4.4 show the first clues of the expected probability of detection for conventional beamforming: In both scenarios (with their particular controllable and environmental conditions) the CDFs associated to P_{ULA} and P_{URA} reach unitary probability for smaller values of power threshold than the other cases of H_{ULA} and H_{URA}. This implies that there could be a smaller probability of detection for power threshold associated to the point where the case $\psi = \theta$ reaches a probability equal to 100%.

Tables 4.1 and 4.2 show the simulated and analytical values of the mean and variance for both ULA and URA cases. As anticipated, simulated and analytical results have slight differences once that our derivations are exact. As a final conclusion, in both cases when steering angle matches the AoA (having the same total number of antennas (M or M_xM_y)) all the PDF, CDF, mean and variance obtain the same values, confirming the analytical derivations. From now on, we will utilize ULA model for discussion once that geometry does not affect the final results.

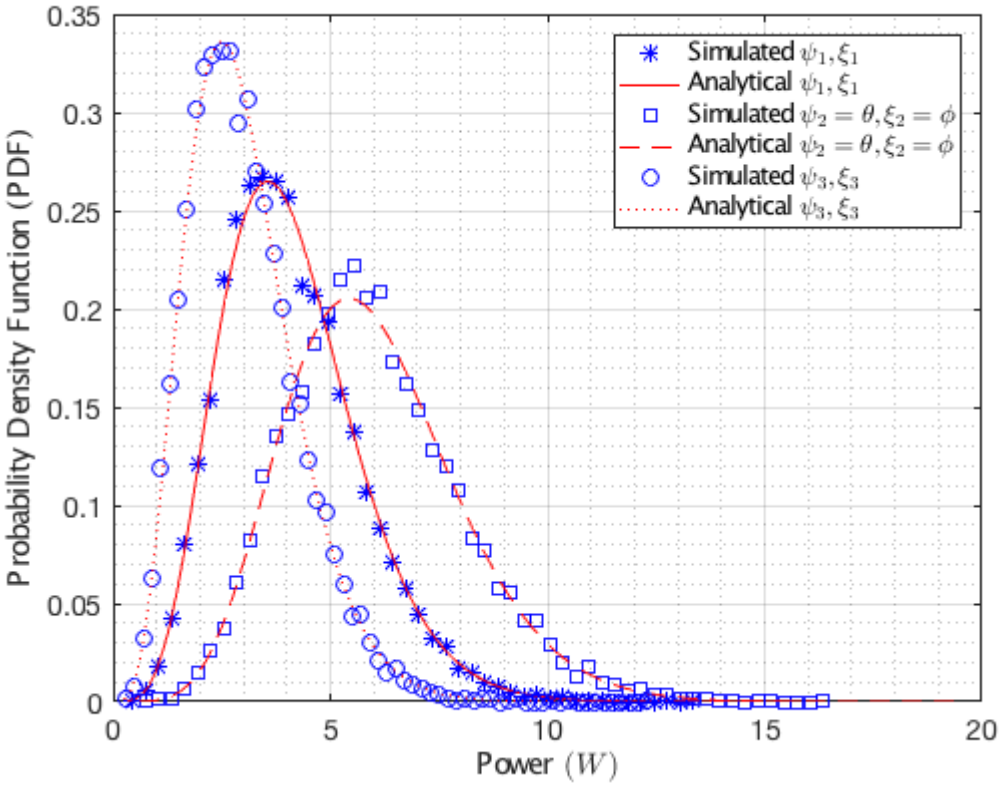

Figure 4.3 – Normalized Histogram for 10^4 realizations of (3.70) and analytical PDF given in (3.75), with $K = 5$, $Mx = 2$, $My = 2$, $L = 1$, $\sigma_f = 1$ and $\sigma_n = 1$ (SNR=0 dB) for $(\psi_1, \xi_1) = (5°, -75°)$, $(\psi_2, \xi_2) = (0°, 30°)$ $(\psi_3, \xi_3) = (40°, 80°)$ in URA case.

	Mean		Variance	
Angle	Simulated	Analytical	Simulated	Analytical
$\psi_1 = 15°$	3.8106	3.822	2.2606	2.2576
$\psi_2 = \theta = 30°$	5.9663	6.0000	3.9974	4.0000
$\psi_3 = 70°$	2.0783	2.0843	0.8628	0.8674

Table 4.1 – Mean and Variance with K=5, L=1, σ_f=1 and σ_n=1 (SNR=0dB) for ULA (M=4) case.

	Mean		Variance	
Angle	Simulated	Analytical	Simulated	Analytical
$\psi_1, \xi_1 = 5°, -75°$	4.0903	4.1044	2.4387	2.4835
$\psi_2 = \theta = 0°, \xi_2 = \psi = 30°$	5.9783	6.0000	3.8820	4.0000
$\psi_3, \xi_3 = 40°, 80°$	2.9858	3.0084	1.6125	1.6067

Table 4.2 – Mean and Variance with K=5, L=1, σ_f=1 and σ_n=1 (SNR=0dB) for URA (M_x=2 and M_y=2) case.

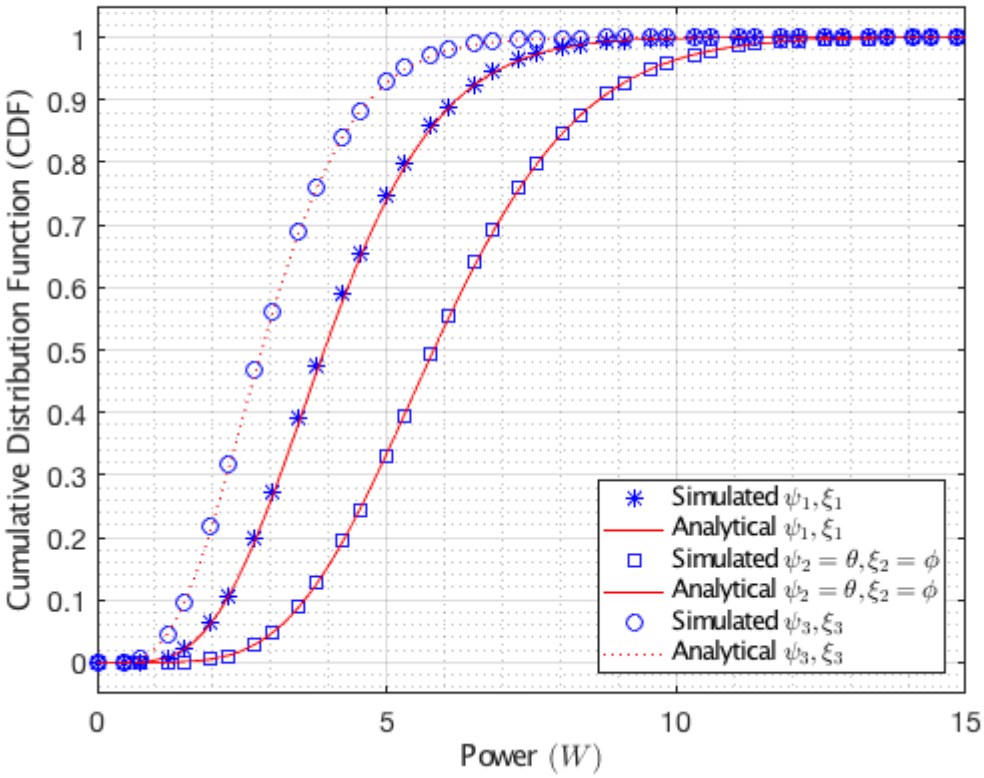

Figure 4.4 – Associated CDF for 10^4 realizations of (3.70) and analytical CDF given in (3.76), with $K = 5$, $Mx = 2$, $My = 2$, $L = 1$, $\sigma_f = 1$ and $\sigma_n = 1$ (SNR=0 dB) for $(\psi_1, \xi_1) = (5°, -75°)$, $(\psi_2, \xi_2) = (0°, 30°)$ $(\psi_3, \xi_3) = (40°, 80°)$ in URA case.

4.2 Cumulative Distribution Function of P_{ULA}

Our model has some controllable parameters (number of snapshots K and number of antennas M) that can compensate the effects of the environmental parameters (fading mean L, noise power σ_n, and fading variance σ_f). This section shows the influence of them in the CDF of P_{ULA} and relates it to the probability of detection.

4.2.1 Influence of the Number of Antennas M

Arrays with a greater number of antennas will receive more signals, therefore the power "sensed" by the spatial filter will be greater. This behavior is confirmed in Fig. 4.5. In other words, the power viewed by a massive MIMO array will be huge, therefore this fact could be used as an advantage for detection.

4.2.2 Influence of the Number of Snapshots K

Fig. 4.6 and Table 4.3 show that the number of snapshots K does not affect the mean of the distribution, but the variance. Fig. 4.6 shows that for low values of the

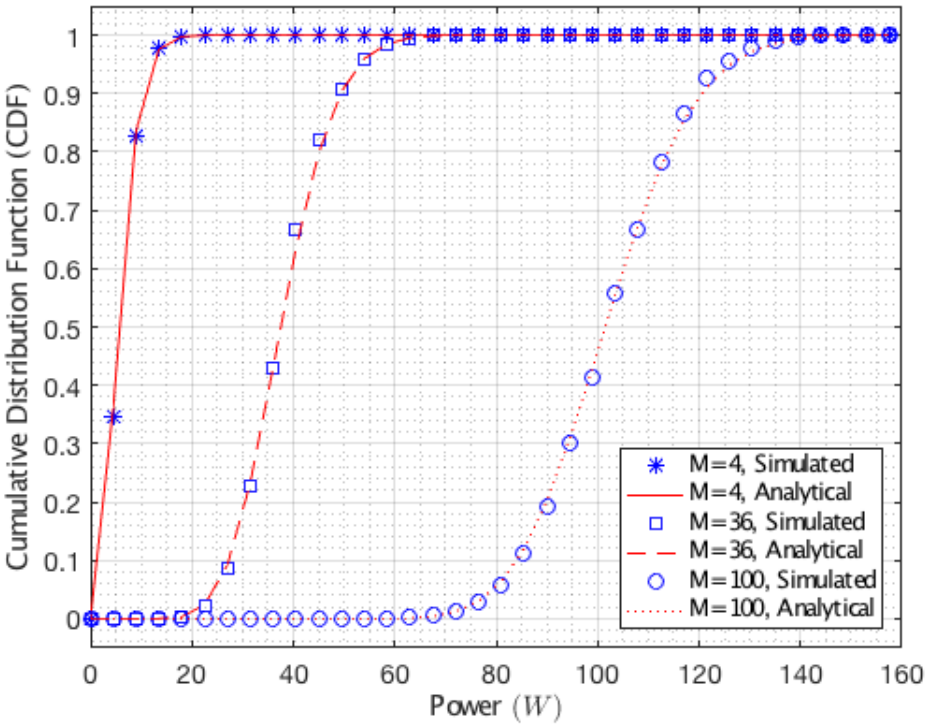

Figure 4.5 – Simulated and Analytical CDF of P_{ULA} with $K = 2$, $L = 1$, $\sigma_f = 1$, and $\sigma_n = 1$ (SNR=0dB).

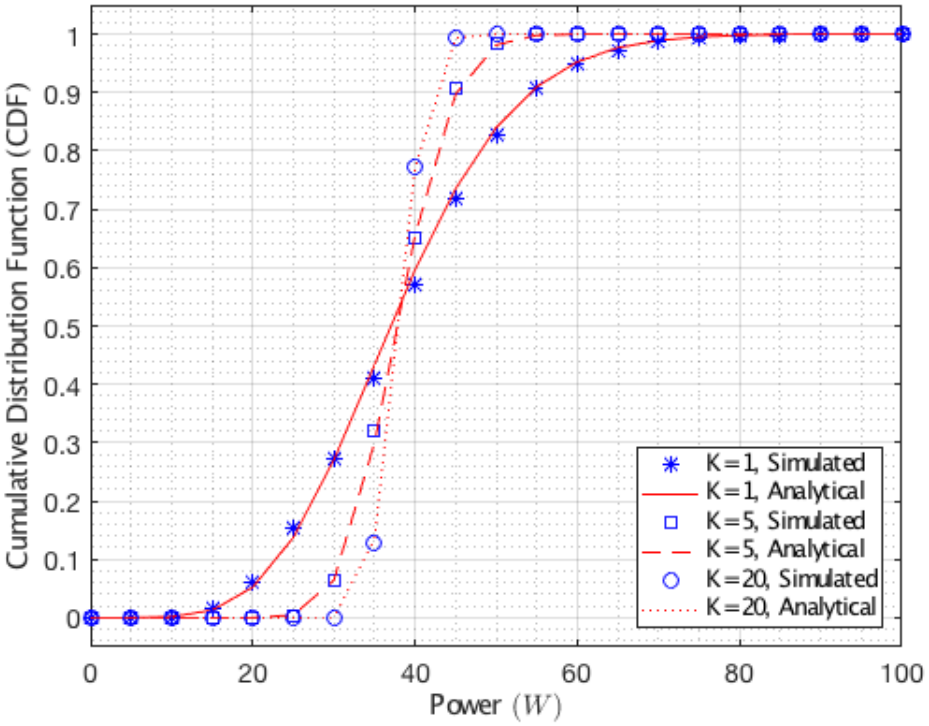

Figure 4.6 – Simulated and Analytical CDF of P_{ULA} with $L = 1$, $M = 36$ $\sigma_f = 1$, and $\sigma_n = 1$ (SNR=0dB).

threshold x, the probability associated with the CDF increases as the number of snapshots K decreases. However, there is a turning point, given exactly by the mean of H_{ULA} in (3.65), where this relation is reversed: the greater the number of snapshots K, the higher the probability associated to the CDF. This behavior implies that correct AoA estimation might be dynamic in this scenario, where the influence of parameters K and noise power σ_n^2 in P_{ULA} is not directly proportional.

	Mean		Variance	
K	Simulated	Analytical	Simulated	Analytical
1	37.9112	38.0000	142.6144	148.0000
5	38.0929	38.0000	30.7504	29.6000
20	38.0266	38.0000	7.7487	7.0000

Table 4.3 – Mean and Variance of P_{ULA} with $L = 1$, $M = 36$ $\sigma_f = 1$, and $\sigma_n = 1$ (SNR=0dB).

4.2.3 Influence of the Fading Standard Deviation σ_f

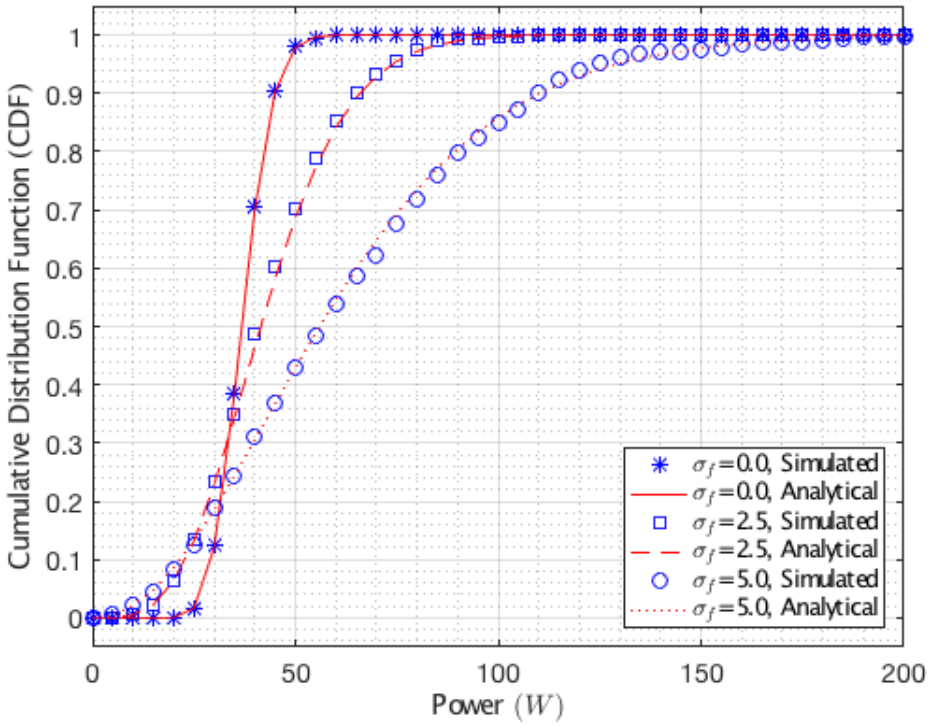

Figure 4.7 – Simulated and Analytical CDF of P_{ULA} with $L = 1$, $K = 2$, $M = 36$ and $\sigma_n = 1$ (SNR=0dB).

Fig. 4.7 exposes a slight difference on distinct values of σ_f for the CDF in small values of power threshold. However, there is a turning point where there is a clear

separation between the curves. This last situation depicts that the perceived power at the array is directly affected by the fading condition, where the probability of detecting a specific threshold is smaller for greater values of σ_f, that is to say, AoA estimation could be wrong for large variance fading situations.

4.2.4 Influence of the fading mean L (LoS component)

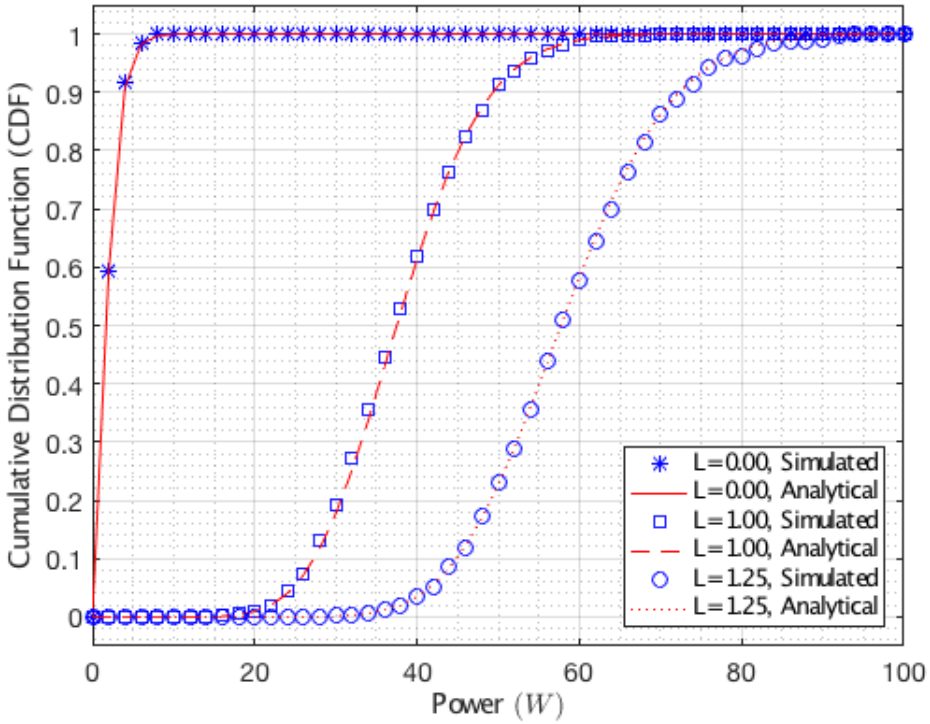

Figure 4.8 – Simulated and Analytical CDF of P_{ULA} with $K = 2$, $M = 36$, $\sigma_f = 1$ and $\sigma_n = 1$ (SNR=0dB).

Fig. 4.8 shows two states of affairs: first, when $L = 0$ (i.e. LoS is null), the CDF attains unitary probability for small values of power threshold. This insinuates that the array will be sensing any type of signal at any time from all possible phenomena like interferences, multi-path propagation, noise, etc. Doubtlessly, the correct AoA estimation could have a lower probability.

Second, the greater the mean of the fading, the smaller the probability for the same values of power threshold. It is implied that the array will sense smaller power values when the fading mean increases, therefore estimation could be wrong.

4.2.5 Influence of the Signal to Noise Ratio SNR(σ_n)

In a similar fashion of the fading scenario, Fig. 4.9 shows the same behavior for the influence of noise power σ_n^2, where there are small differences in the CDF before the

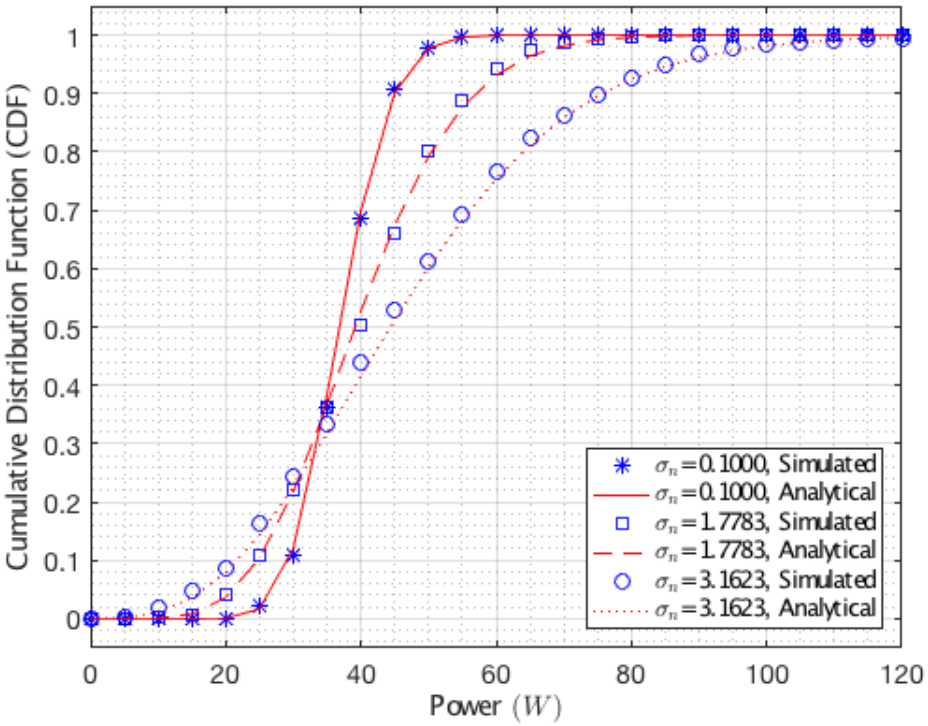

Figure 4.9 – Simulated and Analytical CDF of P_{ULA} with $L = 1$, $K = 2$, $M = 36$ and $\sigma_f = 1$.

turning point. After that threshold, low values of σ_n have more probability to perceive the same power threshold. Once again this performance portrays that AoA estimation could be incorrect by the increase of noise component.

5 Probability of Detection

Probability of Detection Analyses will be done only for ULA configuration, reminding that geometry does not affect the final outcomes of equivalent random variables and associated equations (PDF,CDF, mean and variance). See Chapter 4.

5.1 Derivation

We find the probability of detection for conventional beamforming in a massive MIMO context. Our approach takes advantage of the spatial frequency spectrum characteristics of the conventional beamforming itself.

First, we recall power spatial spectrum equation (3.1) and its random variable equivalences (3.42) and (3.43):

$$H_{ULA}(\psi,\theta) = \frac{\mathbf{a}(\psi)\mathbf{R}\mathbf{a}^H(\psi)}{\mathbf{a}(\psi)\mathbf{a}^H(\psi)} = \frac{\mathbf{a}(\psi)\mathbf{R}\mathbf{a}^H(\psi)}{M}. \tag{5.1}$$

$$H_{ULA_{(\psi,\theta)}} = \frac{\sigma_n^2+\sigma_f^2}{2K}\Omega_{(\psi,\theta)}, \tag{5.2}$$

$$\Omega_{(\psi,\theta)} \sim \chi^2_{nc}\left(2K, \frac{KL^2\left(\pi^2_{1_{(\psi,\theta)}}+\pi^2_{2_{(\psi,\theta)}}\right)}{M\left(\sigma_n^2+\sigma_f^2\right)}\right). \tag{5.3}$$

These equations show that the spatial spectrum depends on the steering angle and the real AoA, in other words, original received signal $\mathbf{r}$ is "transformed" to the spatial frequency domain where the steering angles are the associated spatial frequencies. This fact is illustrated in Fig. 5.1.

Fig 5.1 describes the relation between power and space, where the maximum occurs at $\psi = \theta = 20°$ which is the AoA. Obviously, this is just a specific case, the variation of the other modeled parameters would change this response.

With this situation in context, we define the probability of detection P_D as:

$$P_D = \text{Prob}\left[\hat{\psi} = \theta\right]. \tag{5.4}$$

This circumstance occurs when the power of the associated frequency of $\psi = \theta$ is greater than the power of the rest of steering angles frequencies ψ. In other words, the probability of detection is the probability that P_{ULA} be the maximum of the whole H_{ULA} spectrum, i.e.:

$$P_D = \text{Prob}\left[P_{ULA} > \{H_{ULA_{(\psi_1,\theta)}} \dots H_{ULA_{(\psi_{Q-1},\theta)}}\}\right], \tag{5.5}$$

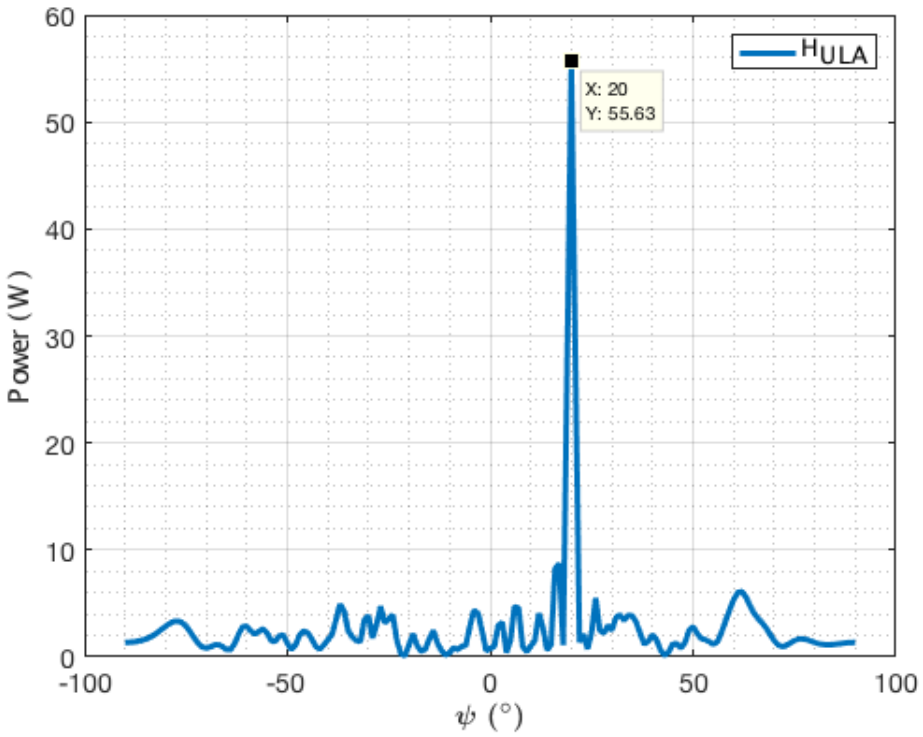

Figure 5.1 – Spatial Power Spectrum of Conventional Beamforming with $\theta = 20°$, K=2, L=1, M=50, $\sigma_n = 1$, $\sigma_f = 1$ for ULA case.

where Q is the number of possible spatial steering frequencies. It is important to emphasize, that in the strict sense, ψ will never be equal to θ since they are real variables. The Probability of Detection is an approach that is valid for a discrete problem and that is the reason for the discretization of ψ.

In order to get an expression, we formulate the detection hypotheses:

- H_0: $H_{ULA_{(\psi,\theta)}}$ has its maximum value at any angle frequency different from the real AoA, that is $\psi \neq \theta$.
- H_1: $H_{ULA_{(\psi,\theta)}}$ has its maximum value at the real AoA, that is $\psi = \theta$.

As it is shown in section 3.1.1, the random variable H_{ULA} defined in (2.11) and (3.1) turns out to be the sum of two squared Gaussian random variables. Each one of these variables corresponds to sum of M Gaussian random variables.

For the hypothesis H_0, that is, for $\psi \neq \theta$, the mean of each Gaussian variate (after unitary variance normalization) will be given by $\frac{\pi_1}{\sqrt{\frac{M\cdot(\sigma_n^2+\sigma_f^2)}{2}}}$, and $\frac{\pi_2}{\sqrt{\frac{M\cdot(\sigma_n^2+\sigma_f^2)}{2}}}$, where π_1 and π_2 are given in (3.44) and (3.45), respectively. As the number of antennas M goes to infinity, $\frac{\pi_1}{\sqrt{\frac{M\cdot(\sigma_n^2+\sigma_f^2)}{2}}}$, and $\frac{\pi_2}{\sqrt{\frac{M\cdot(\sigma_n^2+\sigma_f^2)}{2}}}$ tend to zero. Under this condition, H_{ULA} will be distributed according to a central *Chi*-squared distribution. Therefore, the equivalent

power random variable H_{ULA} (equations (5.2), (5.3)) turns into :

$$H_{ULA} = \frac{\sigma_n^2 + \sigma_f^2}{2K}\Omega_{(\psi,\theta)}, \tag{5.6}$$

where

$$\Omega_{(\psi,\theta)} \sim \chi^2_{nc}\left(2K, \frac{KL^2\left(0^2+0^2\right)}{M\left(\sigma_n^2+\sigma_f^2\right)}\right), \tag{5.7}$$

$$\Omega_{(\psi,\theta)} \sim \chi^2_{nc}\left(2K, \frac{KL^2\cdot 0}{M\left(\sigma_n^2+\sigma_f^2\right)}\right), \tag{5.8}$$

$$\Omega_{(\psi,\theta)} \sim \chi^2_{nc}\left(2K, 0\right), \tag{5.9}$$

$$\Omega_{(\psi,\theta)} \sim \chi^2\left(2K\right). \tag{5.10}$$

where $\Omega_{(\psi,\theta)}$ is a *Chi*-squared distributed random variable with parameter $\kappa = 2K$ (degrees of freedom). Note that equations (5.6) and (5.10) do not have the parameters ψ or θ, which equalizes the associated random variable for all the spatial frequencies different from the AoA ($\psi \neq \theta$). In addition, the associated random variable for the H_0 hypothesis is (coincidentally) exactly the case when there is null LoS, as shown in sub-subsection 3.1.5.2.

The scenario for H_1 indicates that the signals received by the array have the information of the original AoA ($\psi = \theta$), in spite of the fading and noise. Therefore $\pi_1 = M$, and $\pi_2 = -M$. Under this condition, the random variable H_{ULA} will be distributed according to a non-central *Chi*-squared as the one derived in subsection 3.1.4 (equations (3.51), (3.52), and (3.57)):

$$H_{ULA}(\psi = \theta) = P_{ULA} = \frac{\sigma_n^2 + \sigma_f^2}{2K}\Omega_{(\theta,\theta)}, \tag{5.11}$$

where

$$\Omega_{(\theta,\theta)} \sim \chi^2_{nc}\left(2K, \frac{2KML^2}{\sigma_n^2+\sigma_f^2}\right). \tag{5.12}$$

Now, for the hypothesis H_0 case we define the PDF as (reducing from PDF (3.46) and equivalently to (3.67)):

$$f_{H_{ULA}}(x|H_0) = \left(\frac{K}{\sigma_n^2+\sigma_f^2}\right)^K \frac{x^{K-1}e^{-\frac{xK}{\sigma_n^2+\sigma_f^2}}}{\Gamma(K)}, \tag{5.13}$$

where $\Gamma(.)$ is the Gamma function (PAPOULIS; PILLAI, 2002; KAY, 2006).

On the other hand, for the hypothesis H_1 case we define the PDF as (3.58):

$$f_{H_{ULA}}(x|H_1) = f_{P_{ULA}}(x) = \frac{K}{\sigma_n^2+\sigma_f^2}e^{-\frac{K(x+ML^2)}{\sigma_n^2+\sigma_f^2}}\left(\frac{x}{ML^2}\right)^{\frac{K-1}{2}} I_{K-1}\left(\frac{2KL}{\sigma_n^2+\sigma_f^2}\sqrt{Mx}\right), \tag{5.14}$$

where $I_c(d)$ is the modified Bessel function of the first kind with parameters $c \geq 0$ and $d \geq 0$ (PAPOULIS; PILLAI, 2002; KAY, 2006).

It is well known that the probability of a random variable X be smaller than other random variable Y, is defined as (PAPOULIS; PILLAI, 2002; KAY, 2006):

$$\text{Prob}[X < Y] = \int_{-\infty}^{\infty} \left[\int_{-\infty}^{y} f_x(x)dx \right] f_y(y)dy \tag{5.15}$$

In our particular case, we want to know the probability of a $Q-1$ set of i.i.d. random variables being smaller than a unique random variable. Once again, this case is well known and is depicted as (PAPOULIS; PILLAI, 2002; KAY, 2006):

$$\text{Prob}[\{X_1, \ldots, X_{Q-1}\} < Y] = \int_{-\infty}^{\infty} \left[\int_{-\infty}^{y} f_x(x)dx \right]^{Q-1} f_y(y)dy \tag{5.16}$$

In this work, the $Q-1$ associated PDFs are $X_1, X_2, \cdot, X_{Q-1}$ associated to the hypothesis H_0 ($f_{H_{ULA}}(x|H_0)$) and the Y is the variable associated to hypothesis H_1 ($f_{H_{ULA}}(x|H_1)$). Therefore, our Probability of Detection is outlined as:

$$P_D = \text{Prob}[\{H_{ULA_{(\psi_1,\theta)}}, \ldots, H_{ULA_{(\psi_{Q-1},\theta)}}\} < P_{ULA}]$$

$$P_D = \int_0^{\infty} \left[\int_0^{y} \left(\frac{K}{\sigma_n^2 + \sigma_f^2} \right)^K \frac{x^{K-1} e^{-\frac{xK}{\sigma_n^2+\sigma_f^2}}}{\Gamma(K)} dx \right]^{Q-1} \frac{K}{\sigma_n^2 + \sigma_f^2} e^{-\frac{K(y+ML^2)}{\sigma_n^2+\sigma_f^2}} \left(\frac{y}{ML^2} \right)^{\frac{K-1}{2}} I_{K-1}\left(\frac{2KL}{\sigma_n^2 + \sigma_f^2} \sqrt{My} \right) dy \tag{5.17}$$

We get that:

$$\left[\int_0^{y} \left(\frac{K}{\left(\sigma_n^2 + \sigma_f^2\right)} \right)^K \frac{x^{K-1} e^{-\frac{xK}{\left(\sigma_n^2+\sigma_f^2\right)}}}{\Gamma(K)} dx \right] = 1 - \frac{\gamma\left(K, \frac{Ky}{\sigma_n^2+\sigma_f^2}\right)}{\Gamma(K)}, \tag{5.18}$$

where $\gamma(\cdot,\cdot)$ is the incomplete Gamma function, and $\Gamma(\cdot)$ is the gamma function. Recalling the binomial identity:

$$(x+a)^{Q-1} = \sum_{i=0}^{Q-1} \binom{Q-1}{i} x^i a^{Q-1-i}, \tag{5.19}$$

thus (5.17) results on:

$$P_D = \int_0^{\infty} \sum_{i=0}^{Q-1} \binom{Q-1}{i} (-1)^{Q+i-1} \left(\frac{\gamma\left(K, \frac{Ky}{\sigma_n^2+\sigma_f^2}\right)}{\Gamma(K)} \right)^{Q-1-i} \frac{K}{\sigma_n^2 + \sigma_f^2} e^{-\frac{K(y+ML^2)}{\sigma_n^2+\sigma_f^2}} \cdot \left(\frac{y}{ML^2} \right)^{\frac{K-1}{2}} I_{K-1}\left(\frac{2KL}{\sigma_n^2 + \sigma_f^2} \sqrt{My} \right) dy \tag{5.20}$$

Unfortunately, (5.17) does not present a closed form solution, but it is numerically integrable. This will be tested and compared to simulated results in the following section. Although (5.17) is a complex expression, it is easy to implement in mathematical software. Typical processing times take over 50 to 70 ms.

5.2 Numerical Results

5.2.1 Influence of the number of antennas M

Our efforts now focus on the Massive MIMO context, where a huge number of antennas are used for a particular application. So the first results show the influence of the number of antennas in the Probability of Detection as shown in Fig. 5.2.

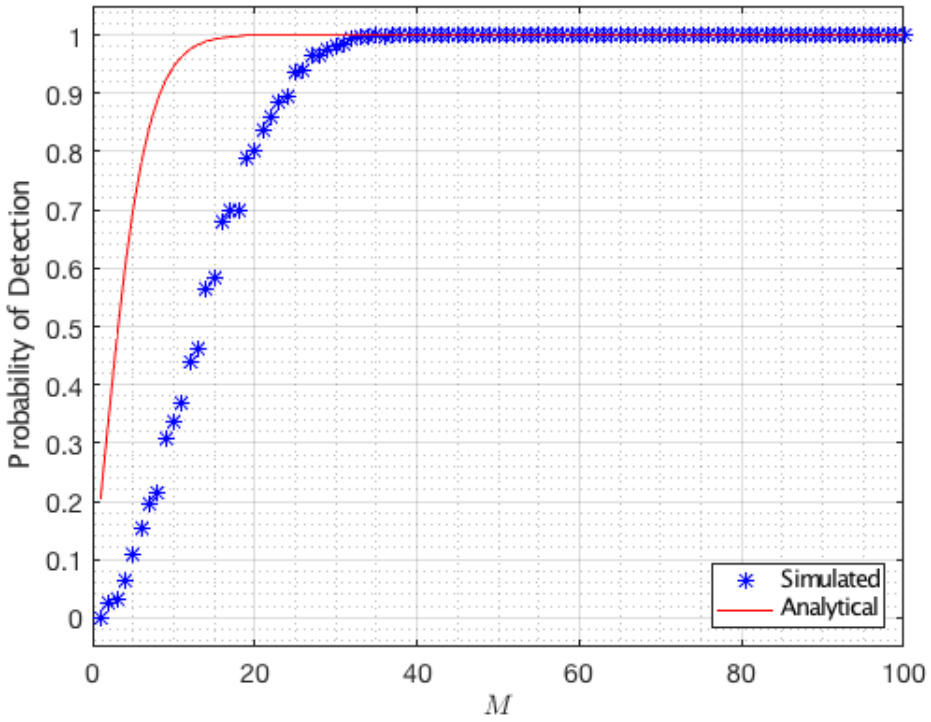

Figure 5.2 – Probability of Detection with, K=2, L=1, Q=121 ($\Delta_\psi = 1.5°$), $\sigma_n = 1$, $\sigma_f = 1$ for ULA case.

As a matter of fact, both simulated and analytical results show a clear tendency: the greater the number of antennas the greater the probability of detection. In other words, the AoA estimation is correct for a large number of antennas. However, the simulated and analytical curves only overlap for high values of M. The assumption for the hypotheses H_0 is that the received signal coming from these Q angles are all independent. To visualize this, let's consider the received signal without noise as

$$\mathbf{r}(t) = \tilde{\mathbf{a}}(\theta) \circ s(t), \tag{5.21}$$

Now we must compute the variable H_{ULA} defined as

$$H_{ULA}(\psi) = \frac{\mathbf{a}_\psi \mathbf{R} \mathbf{a}_\psi^H}{M} = \sum_{k=0}^{K-1} \frac{1}{K} \frac{\mathbf{a}(\psi)\mathbf{a}^H(\theta)\mathbf{a}(\theta)\mathbf{a}(\psi)^H}{M} = \frac{\left|\mathbf{a}(\psi)\mathbf{a}^H(\theta)\right|^2}{M}. \tag{5.22}$$

Remembering that for any ψ, $a(\psi) = [1 \quad e^{j\mu(\psi)} \quad ... \quad e^{j(M-1)\mu(\psi))}]$ where $\mu(\psi) = \frac{2\pi}{\lambda}\Delta\sin(\psi)$, and after proper algebraical/trigonometrical manipulation, the following is obtained:

$$H_{ULA}(\psi) = \frac{\left(\sum_{i=0}^{M-1}\cos\left(i\frac{2\pi\Delta}{\lambda}\Xi\right)\right)^2 + \left(\sum_{i=0}^{M-1}\sin\left(i\frac{2\pi\Delta}{\lambda}\Xi\right)\right)^2}{M}. \tag{5.23}$$

where

$$\Xi = \sin(\psi) - \sin(\theta) \tag{5.24}$$

Note that the variable H_{ULA} will tend to zero as the number of antennas increases, except for:

1. $\Xi = 0$, which implies $\psi = \theta$, i.e. the AoA, as expected.
2. $\Xi = 2$ or $\Xi = -2$, which implies that either ψ or θ are in the extremes of the range $[-\frac{\pi}{2}, \frac{\pi}{2}]$.

Table 5.1 and figure 5.3 bellow show the values for the H_{ULA} as a function of the difference of the sines of the angles $\Xi = \sin(\psi) - \sin(\theta)$. It is possible to observe that $H_{ULA}(\psi \neq \theta)$ is zero for values of M above 5. In short, although the variables might exhibit some dependency, this dependency is negligible as the number of antennas is very high, which is the Massive MIMO case.

Finally, in real life application, a Radio Base Station uses 3 arrays to cover the 2π spatial span. The actual span covered by each array is $\frac{2\pi}{3}$. In other words, the array range will be $[-\frac{\pi}{3}, \frac{\pi}{3}]$, therefore the Ξ range will be $[-1.7, 1.7]$. This fact avoids the maximum condition of the extremes $[-2, 2]$ in H_{ULA} and validates the initial assumptions.

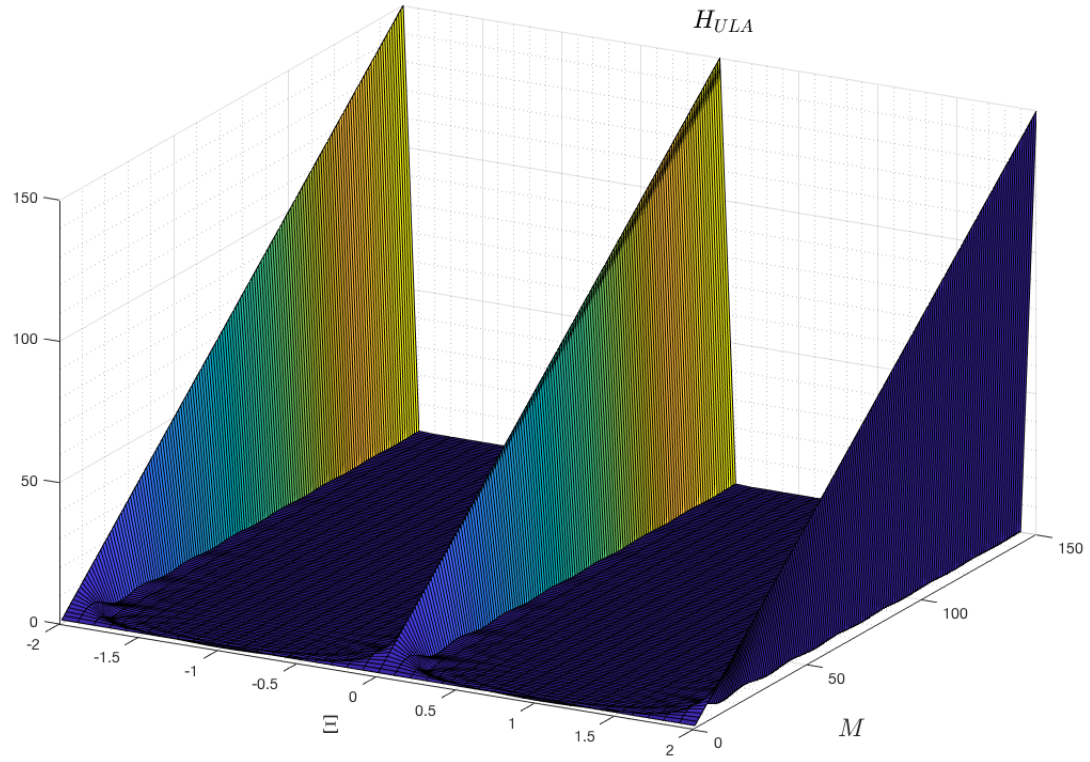

Figure 5.3 – H_{ULA} without noise and fading for different values of Ξ and M.

H_{ULA}	$\Xi = \sin(\psi) - \sin(\theta)$										
M	-2	-1.6	-1.2	-0.8	-0.4	0	0.4	0.8	1.2	1.6	2
4	4	0.25	0.25	0.25	0.25	4	0.25	0.25	0.25	0.25	4
5	5	0.00	0.00	0.00	0.00	5	0.00	0.00	0.00	0.00	5
9	9	0.11	0.11	0.11	0.11	9	0.11	0.11	0.11	0.11	9
16	16	0.06	0.06	0.06	0.06	16	0.06	0.06	0.06	0.06	16
25	25	0.00	0.00	0.00	0.00	25	0.00	0.00	0.00	0.00	25
36	36	0.03	0.03	0.03	0.03	36	0.03	0.03	0.03	0.03	36
49	49	0.02	0.02	0.02	0.02	49	0.02	0.02	0.02	0.02	49
50	50	0.00	0.00	0.00	0.00	50	0.00	0.00	0.00	0.00	50
64	64	0.02	0.02	0.02	0.02	64	0.02	0.02	0.02	0.02	64
75	75	0.00	0.00	0.00	0.00	75	0.00	0.00	0.00	0.00	75
81	81	0.01	0.01	0.01	0.01	81	0.01	0.01	0.01	0.01	81
100	100	0.00	0.00	0.00	0.00	100	0.00	0.00	0.00	0.00	100
121	121	0.01	0.01	0.01	0.01	121	0.01	0.01	0.01	0.01	121
125	125	0.00	0.00	0.00	0.00	125	0.00	0.00	0.00	0.00	125
144	144	0.01	0.01	0.01	0.01	144	0.01	0.01	0.01	0.01	144
150	150	0.00	0.00	0.00	0.00	150	0.00	0.00	0.00	0.00	150

Table 5.1 – H_{ULA} without noise and fading for different values of Ξ and M.

Therefore, our spatial frequency approach is an approximated model and it should be completed for a small number of antennas. In other words, the model shall be extended to a general case, contemplating the "not massive MIMO" operation ($M \leq 50$). This task involves 2 issues:

1. Replace the associated PDF of the H_0 hypotheses (which was modeled as pure noise and fading) by the actual associated PDF of the $Q-1$ spatial frequency equivalent random variables.

2. Due to the dependence between all the Q equivalent random variables of the power spectrum, the hypotheses shall be formulated with the joint PDF in order to get the exact calculation.

5.3 Numerical Results: Normalization by the Parameter M

Note that the received power increases as the number of antennas M increases. In order to make a fair comparison, we will normalize the associated random variables by the number of elements M. Note that when $\psi = \theta$, we get that:

$$P_{ULA} = \sum_{k=0}^{K-1} \frac{1}{K} \frac{\mathbf{a}(\theta)\mathbf{a}^H(\theta)\mathbf{a}(\theta)\mathbf{a}^H(\theta)}{\mathbf{a}(\theta)\mathbf{a}^H(\theta)} = \frac{\mathbf{a}(\theta)\mathbf{a}^H(\theta)\mathbf{a}(\theta)\mathbf{a}^H(\theta)}{\mathbf{a}(\theta)\mathbf{a}^H(\theta)} = \frac{MM}{M} = M. \tag{5.25}$$

It is clear that the parameter M is within the vectors $\mathbf{a}(\theta)$ and $\mathbf{a}(\psi)$ (as their size is $1 \times M$). Thus to normalize the beamforming, we redefine both the steering vector of the AoA and the power spectrum as:

$$\tilde{\mathbf{a}}(\theta) = \frac{\mathbf{a}(\theta)}{\sqrt{M}} = \left[\frac{1}{\sqrt{M}} \quad \frac{e^{j\mu(\theta)}}{\sqrt{M}} \quad \ldots \quad \frac{e^{j(M-1)\mu(\theta))}}{\sqrt{M}}\right], \tag{5.26}$$

$$\tilde{\mathbf{a}}(\psi) = \frac{\mathbf{a}(\psi)}{\sqrt{M}} = \left[\frac{1}{\sqrt{M}} \quad \frac{e^{j\mu(\psi)}}{\sqrt{M}} \quad \ldots \quad \frac{e^{j(M-1)\mu(\psi))}}{\sqrt{M}}\right]. \tag{5.27}$$

Once again, for the perfect case, the received signal vector is a constant, therefore the spatial covariance matrix becomes:

$$\widetilde{\mathbf{R}} = \sum_{k=0}^{K-1} \frac{1}{K} \tilde{\mathbf{a}}^H(\theta)\tilde{\mathbf{a}}(\theta) = \tilde{\mathbf{a}}^H(\theta)\tilde{\mathbf{a}}(\theta), \tag{5.28}$$

then the conventional beamforming changes into:

$$\widetilde{H}_{ULA}(\psi) = \sum_{k=0}^{K-1} \frac{1}{K} \frac{\tilde{\mathbf{a}}(\psi)\ \tilde{\mathbf{a}}^H(\theta)\tilde{\mathbf{a}}(\theta)\tilde{\mathbf{a}}^H(\psi)}{\tilde{\mathbf{a}}(\psi)\tilde{\mathbf{a}}^H(\psi)} = \frac{\frac{\mathbf{a}(\psi)}{\sqrt{M}}\frac{\mathbf{a}^H(\theta)}{\sqrt{M}}\frac{\mathbf{a}(\theta)}{\sqrt{M}}\frac{\mathbf{a}^H(\psi)}{\sqrt{M}}}{\frac{\mathbf{a}(\psi)}{\sqrt{M}}\frac{\mathbf{a}^H(\psi)}{\sqrt{M}}} = \frac{1}{M}\frac{\mathbf{a}(\psi)\ \mathbf{a}^H(\theta)\mathbf{a}(\theta)\mathbf{a}^H(\psi)}{\mathbf{a}(\psi)\mathbf{a}^H(\psi)}. \tag{5.29}$$

Consequently, for the special case $\psi = \theta$, we get that:

$$\widetilde{P}_{ULA} = \sum_{k=0}^{K-1} \frac{1}{K} \frac{1}{M} \frac{\mathbf{a}(\theta)\mathbf{a}^H(\theta)\mathbf{a}(\theta)\mathbf{a}^H(\theta)}{\mathbf{a}(\theta)\mathbf{a}^H(\theta)} = \frac{1}{M} P_{ULA} = \frac{M}{M} = 1, \tag{5.30}$$

where finally the power spectrum signal is normalized.

As a statement of the obvious, the normalization modifies all the equations of the complete detection problem and its hypotheses. Consequently, we are going to show the equations that serve our particular interest. The new associated random variable of the hypotheses H_0 and H_1 become (after simplification):

$$\widetilde{H}_{ULA_{(\psi,\theta)}} = \frac{M\sigma_n^2 + \sigma_f^2}{2KM} \widetilde{\Omega}_{(\psi,\theta)}, \tag{5.31}$$

where

$$\widetilde{\Omega}_{(\psi,\theta)} \sim \chi^2 (2K). \tag{5.32}$$

and

$$\widetilde{H}_{ULA}(\psi = \theta) = \widetilde{P}_{ULA} = \frac{M\sigma_n^2 + \sigma_f^2}{2KM} \widetilde{\Omega}_{(\theta,\theta)}, \tag{5.33}$$

where

$$\widetilde{\Omega}_{(\theta,\theta)} \sim \chi^2_{nc} \left(2K, \frac{2KML^2}{M\sigma_n^2 + \sigma_f^2}\right). \tag{5.34}$$

Eventually, the new associated PDFs of the hypotheses are stated as:

$$f_{\widetilde{H}_{ULA}}(x|H_0) = \left(\frac{KM}{M\sigma_n^2 + \sigma_f^2}\right)^K \frac{x^{K-1} e^{-\frac{xKM}{M\sigma_n^2 + \sigma_f^2}}}{\Gamma(K)}, \tag{5.35}$$

where $\Gamma(.)$ is the Gamma function (PAPOULIS; PILLAI, 2002; KAY, 2006), and

$$f_{\widetilde{H}_{ULA}}(x|H_1) = f_{\widetilde{P}_{ULA}}(x) = \frac{KM}{M\sigma_n^2 + \sigma_f^2} e^{-\frac{KM(x+L^2)}{M\sigma_n^2 + \sigma_f^2}} \left(\frac{x}{L^2}\right)^{\frac{K-1}{2}} I_{K-1}\left(\frac{2KML}{M\sigma_n^2 + \sigma_f^2}\sqrt{x}\right), \tag{5.36}$$

where $I_c(d)$ is the modified Bessel function of the first kind with parameters $c \geq 0$ and $d \geq 0$ (PAPOULIS; PILLAI, 2002; KAY, 2006). Finally we get the new probability of detection:

$$\widetilde{P}_D = \text{Prob}[\{\widetilde{H}_{ULA_{(\psi_1,\theta)}}, \ldots, \widetilde{H}_{ULA_{(\psi_{Q-1},\theta)}}\} < \widetilde{P}_{ULA}] =$$

$$\widetilde{P}_D = \int_0^\infty \sum_{i=0}^{Q-1} \binom{Q-1}{i} (-1)^{Q+i-1} \left(\frac{\gamma\left(K, \frac{KMy}{M\sigma_n^2 + \sigma_f^2}\right)}{\Gamma(K)}\right)^{Q-1-i} \cdot \frac{KM}{M\sigma_n^2 + \sigma_f^2} \cdot e^{-\frac{KM(y+L^2)}{M\sigma_n^2 + \sigma_f^2}} \cdot \left(\frac{y}{L^2}\right)^{\frac{K-1}{2}} I_{K-1}\left(\frac{2KML}{M\sigma_n^2 + \sigma_f^2}\sqrt{y}\right) dy \tag{5.37}$$

Once again, equation (5.37) has not a closed form expression but it is numerically integrable.

5.3.1 Influence of the number of antennas M

The new derived probability of detection is evaluated variating the number of antennas M and compared to simulated results, as shown in Fig. 5.4.

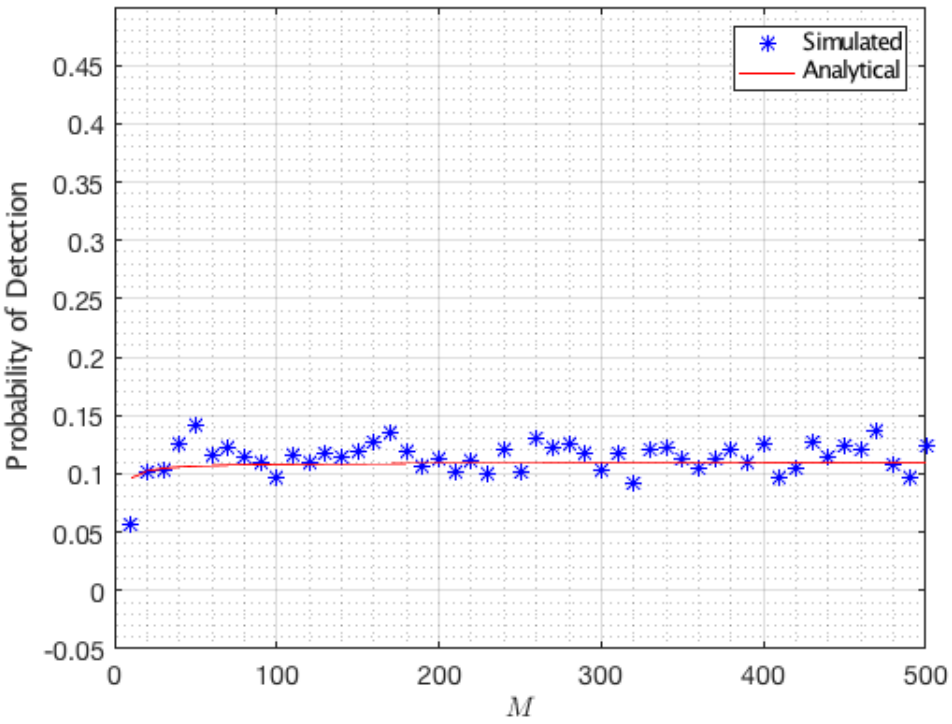

Figure 5.4 – Probability of Detection with, K=2, L=1, Q=121 ($\Delta_\psi = 1.5°$), $\sigma_n = 1$, $\sigma_f = 1$ for ULA case.

Fig. 5.4 shows that $\widetilde{P}_D$ is barely affected by the parameter M, as desired. Also note that there is a perfect match of simulated and analytical outcomes for all the range that is considered massive MIMO ($M \geq 50$).

5.3.2 Influence of the number of snapshots K

Fig. 5.5 depicts a clear relation: the greater the number of snapshots K the greater the probability of detection $\widetilde{P}_D$. This behavior is expected considering that the as the number of snapshots increases, the conventional beamformer has more information of the signal. Therefore it can perform a better estimation. Also, analytical and simulated curves are very close, with small differences.

5.3.3 Influence of noise standard deviation σ_n

Fig. 5.6 depicts another expected performance: the greater the power of noise σ_n^2 the smaller the probability of detection $\widetilde{P}_D$. Definitely, any estimator receiving signals

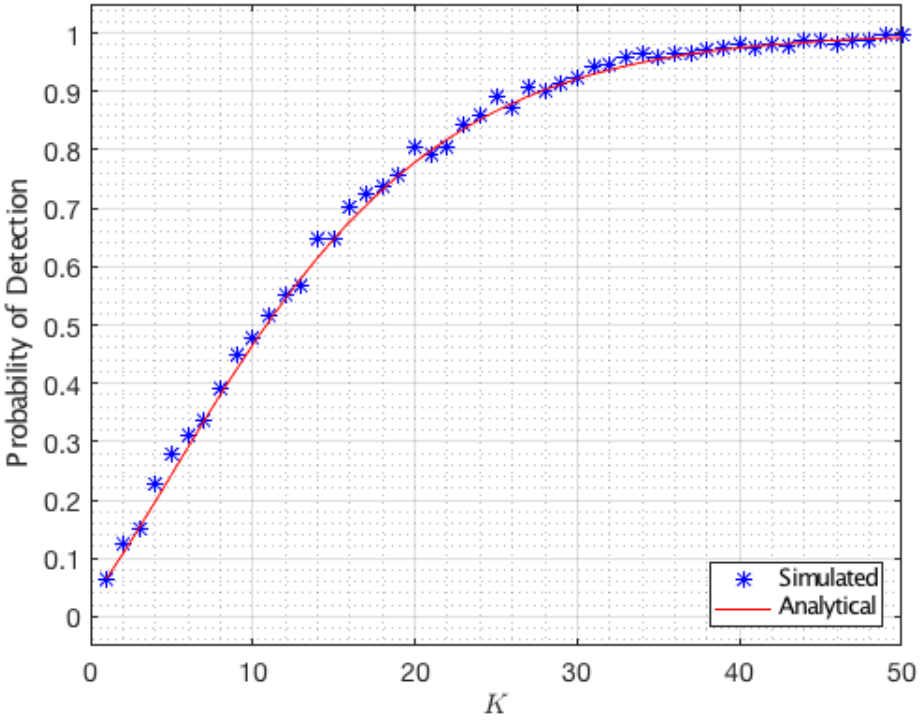

Figure 5.5 – Probability of Detection with, L=1, M=100, Q=121 ($\Delta_\psi = 1.5°$), $\sigma_n = 1$, $\sigma_f = 1$ for ULA case.

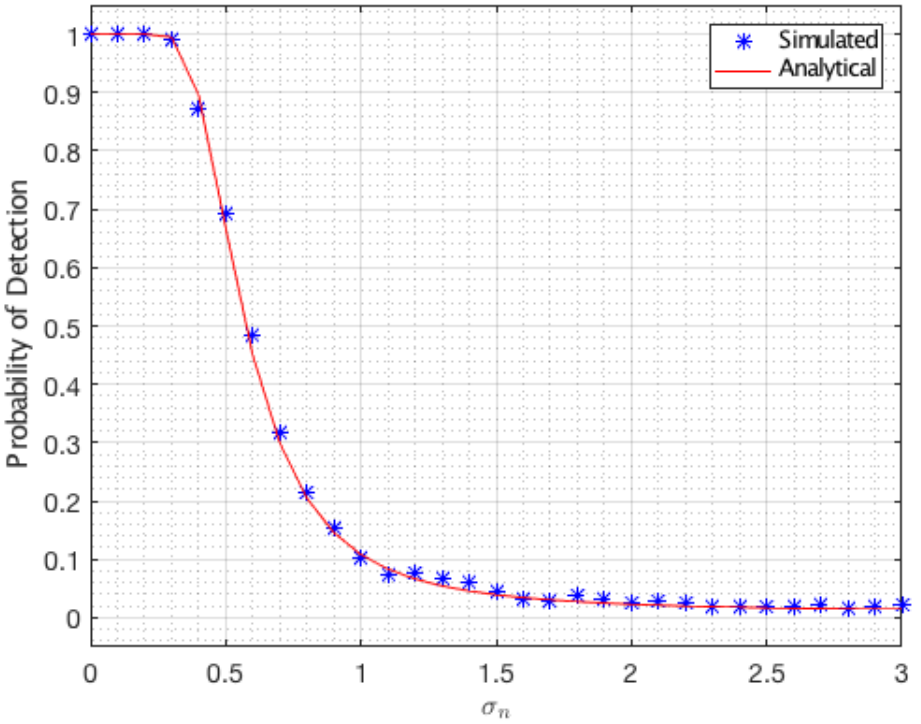

Figure 5.6 – Probability of Detection with, K=2, L=1, M=100, Q=121 ($\Delta_\psi = 1.5°$), $\sigma_f = 1$ for ULA case.

with huge noise power will misbehave, therefore the AoA estimation would be incorrect. In this particular simulated case, the absence of noise gives a unitary probability of detection, portraying that the controllable parameters (K and M) overcome the fading phenomenon (L and σ_f).

5.3.4 Influence of the Fading Standard Deviation σ_f

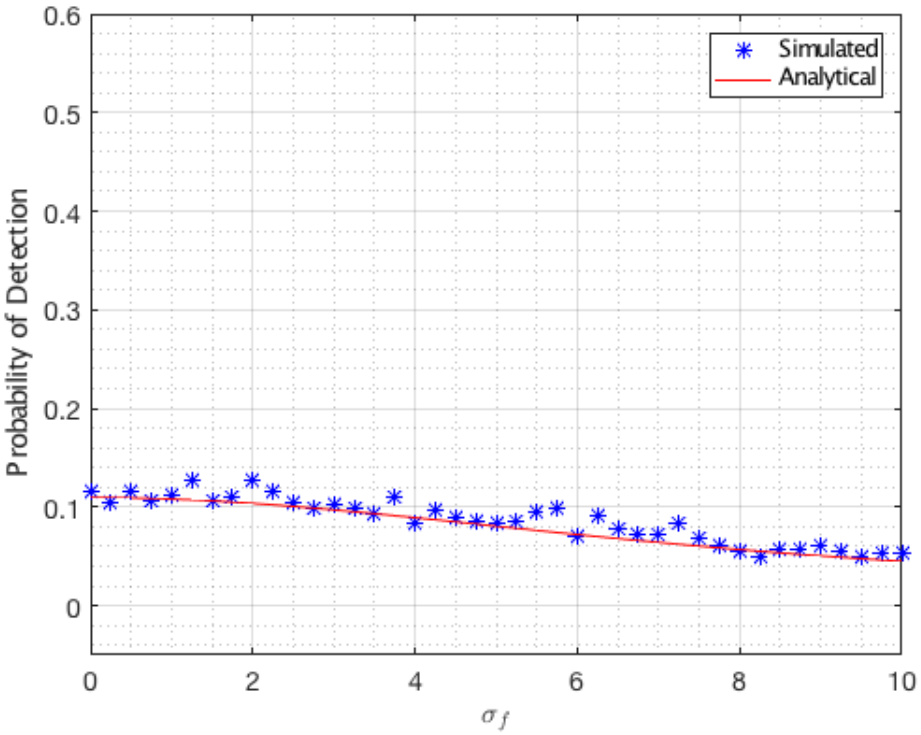

Figure 5.7 – Probability of Detection with, K=2, L=1, M=100, Q=121 ($\Delta_\psi = 1.5°$), $\sigma_n = 1$, for ULA case.

An increase in the fading standard deviation σ_f decreases the probability of detection $\widetilde{P}_D$, as shown in Fig. 5.7. This result is presumable, higher values of σ_f imply higher values of randomness associated with the AoA information present in the received signal, boosting the error of any estimator. In this specific result, in spite of the high variability of σ_f, this parameter has the smaller influence on the $\widetilde{P}_D$ outcome. Clearly, the other parameters have more influence.

5.3.5 Influence of Fading Mean L (LoS component)

Fig. 5.8 reveals that greater values of fading mean L (LoS component) improve the probability of detection. This tendency can be explicated by our model: parameter L (LoS component) multiplies directly the AoA steering vector, increasing the power of the signal. Hence it "strengthens" the AoA information in contrast to the "weakening" of other

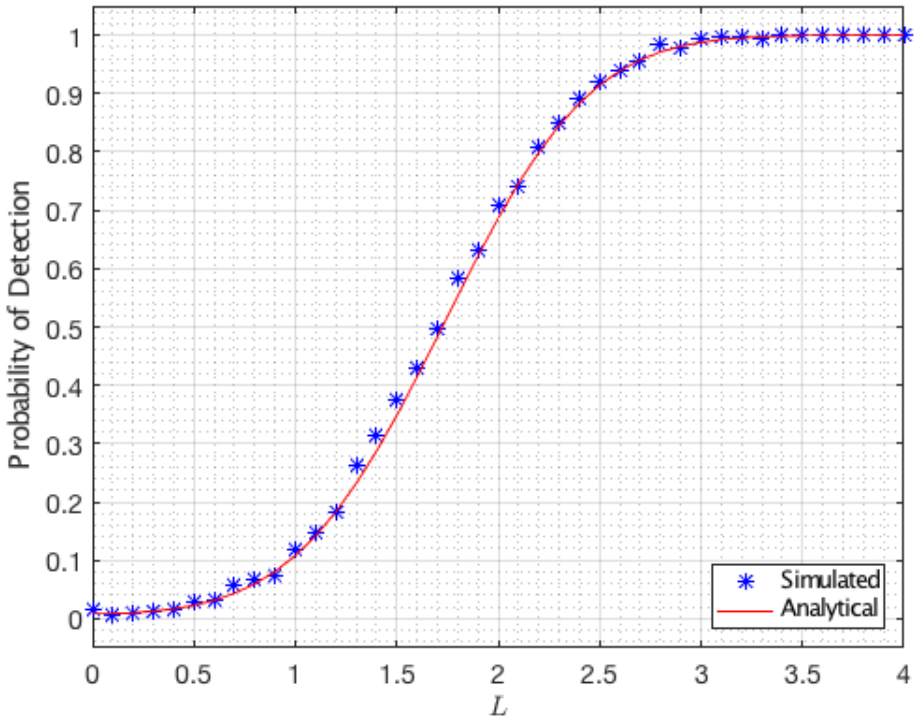

Figure 5.8 – Probability of Detection with, K=2, M=100, Q=121 ($\Delta_\psi = 1.5°$), $\sigma_n = 1$, $\sigma_f = 1$ for ULA case.

phenomena. However, this is a misleading result, because L (LoS component) is part of a two-parameter phenomenon: fading, where a great σ_f could worsen the detection.

5.3.6 Influence of the number of steering angles Q

Resolution determines the level of detail of a measured variable. In our case, the resolution is the angle step between the possible steering angles chosen to describe the AoA spatial spectrum. According to beamforming principles, there is a maximum angular resolution that can be achieved for proper signal array processing (RICHARDS, 2005). This maximum is the denominated $3dB$ beamwidth:

$$\Delta_{3dB} = \Delta_\psi = \frac{2}{M}, \tag{5.38}$$

which is given in radians. This approximation is set for isotropic antennas, large number of antennas, and antenna spacing equal to $d = \frac{\lambda}{2}$ conditions, as stated in section 2.1. Now putting this statement on our application, we define:

$$Q = \frac{S}{\Delta_\psi}, \tag{5.39}$$

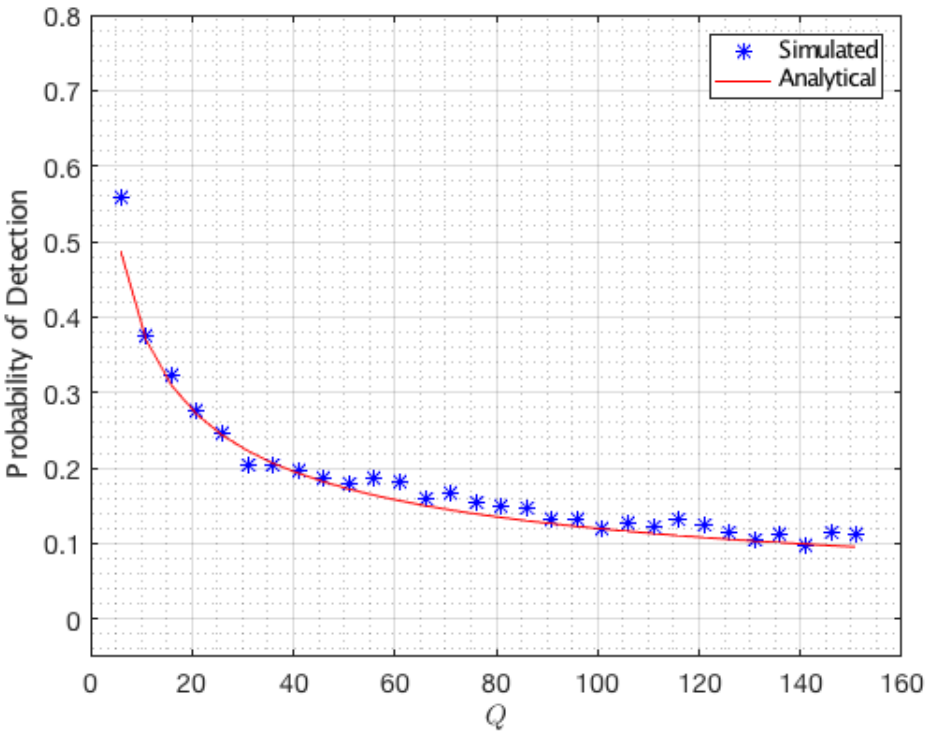

Figure 5.9 – Probability of Detection with, K=2, L=1, M=100, $\sigma_n = 1$, $\sigma_f = 1$ for ULA case.

where S is the span of the steering angles. In our case the range is set as $\{-\frac{\pi}{2}$ to $\frac{\pi}{2}\}$ in order to avoid angle ambiguity in the estimation. Thus:

$$Q = \frac{\frac{\pi}{2} - \left(-\frac{\pi}{2}\right)}{\Delta_\psi} = \frac{\pi}{\Delta_\psi}, \tag{5.40}$$

so finally, replacing (5.38) as a maximum condition:

$$Q < \frac{\pi}{2} M. \tag{5.41}$$

In the simulation scenario , we established $M = 100$, therefore $Q < 157.07$. Previous results shown in subsections 5.3.2, 5.3.3, 5.3.4, and 5.3.5, considered this restriction for simulation and analyses developments. For scenarios exposed in subsections 5.2.1 and 5.3.1, this restriction was liberated, in order to make a fair comparison of the influence of the number of antennas.

It is predictable that the vaster the number of Q the smaller the $\widetilde{P}_D$ because there is a greater chance to miss the correct angle. Fig. 5.9 agrees with the previous statement and shows that for a higher number of Q there are few differences in $\widetilde{P}_D$ performance. In terms of probability if we want to eliminate the error induced by the discretization we shall make Q tend to ∞. However, the Q frequencies represent the size of the alphabet of the steering angles, and by probability theory, a distribution with a ∞

size of alphabet becomes a continuous distribution. Therefore the probability associated with an element of the alphabet is equal to 0. In other words, if we eliminate discretization our metric (P_D) will be useless. Hence, there is a practical limit in discretization that gives sufficient information about the problem and prevents the use of unnecessary extra computational resources. To sum up, there is a trade-off between precision and detection.

Conclusions

We have derived the exact analytical probability of detection for conventional beamforming on ULA and URA geometries considering fading and noise scenarios in a massive MIMO context. The resulting equation is related to a scaled non-central *Chi-squared* random variable and its associated PDF and CDF. Our simulated and analytical curves matched perfectly, corroborating the analytical derivations.

The number of snapshots, K, and the number of antennas, M, impacted directly the probability of detection and therefore the estimation angle. These parameters can mitigate the effects of fading and noise. Particularly, in conventional beamforming, a large number of antennas improved the probability of detection, useful justification for Massive MIMO technique application.

Parameter K did not affect the mean, but the variance of associated random variable H_{ULA}. The absence of the fading mean (LoS) made the random variable H_{ULA} very dependent on K, fading variance, and noise characteristics. Consequently, conventional beamforming with arrays becomes useless for angle estimation (i.e. the probability of detection tends to be null). The probability of detection was directly affected by the dedicated number of steering frequencies Q: the higher the Q, the worse the estimation.

The probability of Detection for URA geometry behaved in a similar fashion as ULA geometry, where all associated modeled equations change the parameter M by the M_xM_y product. This issue confirms previous known advantages of URA geometry over ULA geometry: the possibility of 3D AoA estimation (elevation and azimuth angles) and spatial efficiency for a massive number of antennas.

Conclusively, the proposed probability of detection metric depicted two primary benefits: showed some behavior issues for existent algorithms not exposed by other metrics and unfolded a new way for research in the complex multivariate statistics.

Future work

Future work could extend this framework considering other array layouts such as fractal, Uniform Circular Array (UCA) or Uniform Cylindrical Array (UCyA).

Previous thesis deductions could be extended to a general case: Detect multiple dedicated signals at the antenna array.

Analytical derivations of probabilities of detection for other power spectrum based algorithms like Capon (CAPON, 1969) and MUSIC (SCHMIDT, 1986) are proposed as future work in order to set forth new difficult mathematical developments (non-central complex Wishart matrices and complex eigenvectors PDFs equivalences).

The derivation of the probability of detection for any number of antennas M (outside the Massive MIMO condition) could be set for the general model.

Finally, the new probability of detection metric could be derived and assessed by deepening the fading channel using generalizing distributions such as $\kappa - \mu$, $\eta - \mu$ (YACOUB, 2007b) and $\alpha - \mu$ (YACOUB, 2007a) models.

Publications

The results from this work were condensed as a paper and submitted to the **IEEE Access Multidisciplinary Open Access Journal**.
The article was named as "*Probability of Detection of the Angle of Arrival for Massive MIMO Arrays*" and was accepted for publication with Digital Object Identifier (DOI): 10.1109/ACCESS.2018.2877364.

Bibliography

BECK, A.; STOICA, P.; LI, J. Exact and approximate solutions of source localization problems. *IEEE Transactions on Signal Processing*, v. 56, n. 5, p. 1770–1778, May 2008. ISSN 1053-587X. Cited 2 times on pages 17 and 18.

CAPON, J. High-resolution frequency-wavenumber spectrum analysis. *Proceedings of the IEEE*, v. 57, n. 8, p. 1408–1418, Aug 1969. ISSN 0018-9219. Cited 3 times on pages 18, 24, and 66.

CHEN, Z.; GOKEDA, G.; YU, Y. *Introduction to Direction-of-arrival Estimation*. 1. ed. [S.l.]: Artech House, 2010. (Artech House Remote Sensing Library). ISBN 9781596930896. Cited 10 times on pages , 17, 18, 20, 21, 23, 24, 25, 26, and 28.

DARDARI, D.; CHONG, C. C.; WIN, M. Threshold-based time-of-arrival estimators in uwb dense multipath channels. *IEEE Transactions on Communications*, v. 56, n. 8, p. 1366–1378, August 2008. ISSN 0090-6778. Cited on page 17.

FAN, Y.; LI, J. B.; LI, H.; TIAN, C. A stochastic framework of millimeter wave signal for mobile users: Experiment, modeling and application in beam tracking. In: *2018 11th Global Symposium on Millimeter Waves (GSMM)*. [S.l.: s.n.], 2018. p. 1–6. Cited 2 times on pages 17 and 18.

FANG, S. H.; WANG, C. H. A dynamic hybrid projection approach for improved wi-fi location fingerprinting. *IEEE Transactions on Vehicular Technology*, v. 60, n. 3, p. 1037–1044, March 2011. ISSN 0018-9545. Cited on page 17.

GARCIA, N.; WYMEERSCH, H.; LARSSON, E. G.; HAIMOVICH, A. M.; COULON, M. Direct localization for massive MIMO. *IEEE Transactions on Signal Processing*, v. 65, n. 10, p. 2475–2487, May 2017. ISSN 1053-587X. Cited on page 17.

GREENE, R. *Las 33 Estrategias de la Guerra*. 1. ed. [S.l.]: Editorial Océano de México, 2007. ISBN 9789707772441. Cited on page 6.

HE, Y. L. B. Array signal processing for maximum likelihood direction-of-arrival estimation. *Journal of Electrical & Electronic Systems*, v. 03, 01 2014. Cited 2 times on pages 17 and 18.

JONG, Y. L. C. D.; HERBEN, M. H. A. J. High-resolution angle-of-arrival measurement of the mobile radio channel. *IEEE Transactions on Antennas and Propagation*, v. 47, n. 11, p. 1677–1687, Nov 1999. ISSN 0018-926X. Cited on page 23.

KAY, S. *Intuitive Probability and Random Processes using MATLAB*. 1. ed. [S.l.]: Springer US, 2006. ISBN 9780387241579. Cited 3 times on pages 52, 53, and 58.

KHAN, M. W.; SALMAN, N.; KEMP, A. H. Cooperative positioning using angle of arrival and time of arrival. In: *2014 Sensor Signal Processing for Defence (SSPD)*. [S.l.: s.n.], 2014. p. 1–5. Cited on page 17.

KRIM, H.; VIBERG, M. Two decades of array signal processing research: the parametric approach. *IEEE Signal Processing Magazine*, v. 13, n. 4, p. 67–94, Jul 1996. ISSN 1053-5888. Cited on page 20.

KWAKKERNAAT, M. R. J. A. E.; JONG, Y. L. C. de; BULTITUDE, R. J. C.; HERBEN, M. H. A. J. High-resolution angle-of-arrival measurements on physically-nonstationary mobile radio channels. *IEEE Transactions on Antennas and Propagation*, v. 56, n. 8, p. 2720–2729, Aug 2008. ISSN 0018-926X. Cited on page 23.

LARSSON, E. G.; EDFORS, O.; TUFVESSON, F.; MARZETTA, T. L. Massive MIMO for next generation wireless systems. *IEEE Communications Magazine*, v. 52, n. 2, p. 186–195, February 2014. ISSN 0163-6804. Cited 3 times on pages 17, 18, and 24.

MARZETTA, T. L. Noncooperative cellular wireless with unlimited numbers of base station antennas. *IEEE Transactions on Wireless Communications*, v. 9, n. 11, p. 3590–3600, November 2010. ISSN 1536-1276. Cited 3 times on pages 17, 18, and 24.

MUIRHEAD, R. J. *Aspects of Multivariate Statistical Theory*. 2. ed. [S.l.]: John Wiley & Sons, 2005. ISBN 9780471769859. Cited on page 18.

PAPOULIS, A.; PILLAI, S. *Probability, Random Variables, and Stochastic Processes*. 4. ed. [S.l.]: McGraw-Hill, 2002. (McGraw-Hill electrical and electronic engineering series). ISBN 9780073660110. Cited 5 times on pages 34, 40, 52, 53, and 58.

RICHARDS, M. *Fundamentals of Radar Signal Processing*. Mcgraw-hill, 2005. (Professional Engineering). ISBN 9780071444743. Disponível em: <https://books.google.com.br/books?id=VOvsJ7G1oDEC>. Cited on page 62.

ROY, R.; KAILATH, T. Esprit-estimation of signal parameters via rotational invariance techniques. *IEEE Transactions on Acoustics, Speech, and Signal Processing*, v. 37, n. 7, p. 984–995, Jul 1989. ISSN 0096-3518. Cited on page 18.

SALMI, J.; MOLISCH, A. F. Propagation parameter estimation, modeling and measurements for ultrawideband mimo radar. *IEEE Transactions on Antennas and Propagation*, v. 39, p. 4257–4267, 11 2011. Cited on page 18.

SAVIC, V.; LARSSON, E. G. Fingerprinting-based positioning in distributed massive mimo systems. In: *2015 IEEE 82nd Vehicular Technology Conference (VTC2015-Fall)*. [S.l.: s.n.], 2015. p. 1–5. Cited on page 17.

SCHMIDT, R. Multiple emitter location and signal parameter estimation. *IEEE Transactions on Antennas and Propagation*, v. 34, n. 3, p. 276–280, Mar 1986. ISSN 0018-926X. Cited 4 times on pages 18, 25, 26, and 66.

WANG, M. J.; CAI, J. L.; TSENG, F. S.; HSU, C. Y. A low-complexity 2-D angle of arrival estimation in massive mimo systems. In: *2016 International Computer Symposium (ICS)*. [S.l.: s.n.], 2016. p. 710–713. Cited 2 times on pages 17 and 18.

XU, G.; ROY, R. H.; KAILATH, T. Detection of number of sources via exploitation of centro-symmetry property. *IEEE Transactions on Signal Processing*, v. 42, n. 1, p. 102–112, Jan 1994. ISSN 1053-587X. Cited on page 23.

XU, L.; WANG, J.; ZHANG, H.; GULLIVER, T. A. Performance analysis of iaf relaying mobile d2d cooperative networks. *Journal of the Franklin Institute*, v. 354, n. 2, p. 902 – 916, 2017. ISSN 0016-0032. Disponível em: <http://www.sciencedirect.com/science/article/pii/S0016003216303908>. Cited on page 17.

XU, L.; ZHANG, H.; WANG, J.; GULLIVER, T. A. Joint tas/sc and power allocation for iaf relaying d2d cooperative networks. *Wireless Networks*, v. 23, p. 2135–2143, 2017. Cited on page 17.

YACOUB, M. D. The α - μ distribution: A physical fading model for the stacy distribution. *IEEE Transactions on Vehicular Technology*, v. 56, n. 1, p. 27–34, Jan 2007. ISSN 0018-9545. Cited on page 66.

YACOUB, M. D. The κ - μ distribution and the η-μ distribution. *IEEE Antennas and Propagation Magazine*, v. 49, n. 1, p. 68–81, Feb 2007. ISSN 1045-9243. Cited on page 66.

ZEYTINCI, M. B.; SARI, V.; HARMANCI, F. K.; ANARIM, E.; AKAR, M. Location estimation using RSS measurements with unknown path loss exponents. *EURASIP Journal on Wireless Communications and Networking*, v. 2013, n. 1, p. 178, Jun 2013. ISSN 1687-1499. Disponível em: <https://doi.org/10.1186/1687-1499-2013-178>. Cited on page 17.

ZHANG, L.; CHEW, Y. H.; WONG, W. C. A novel angle-of-arrival assisted extended kalman filter tracking algorithm with space-time correlation based motion parameters estimation. In: *2013 9th International Wireless Communications and Mobile Computing Conference (IWCMC)*. [S.l.: s.n.], 2013. p. 1283–1289. ISSN 2376-6492. Cited 2 times on pages 17 and 18.